JOURNAL OF MULTIFUNCTIONAL MATERIALS & PHOTOSCIENCE
8(1), June 2017, pp. 61-107

Advancements in the Development of Graphene Nanocomposites for Dye-sensitized Solar Cells (DSSC) Applications

Yonrapach Areerob, Won-Chun Oh*

Department of Advanced Materials Science & Engineering, Hanseo University, Chungnam 356-706, South Korea

Abstract: Dye sensitized solar cells (DSSCs) are widely studied for the safe and reliable energy supply. Due to its low fabrication cost, eco-friendly production and competitive efficiency, this is the promising technology. The incorporation of graphene-based materials into solar cell represents a cost-effective option to boost its stability, optical transmittance and the overall performance. Graphene has been used as transparent window and counter electrodes, interface layers, hole/electron transport material and also as a buffer layer to slow-down charge recombination in solar cell. This review will focus on recent advances in graphenes and their application as materials to improve the photovoltaic performance of DSSCs. Promising properties of graphene has shown to enhance various layers of a solar cell. Although layer-by-layer chemical process can detach sections of graphene, this can be improved by doping. Conversion of graphite to graphene enhances the conductivity of photo excited electrons, electron mobility and reduces the recombination rate of electron/hole pairs. The tunable bandgap properties and excellent thermal and mechanical stability of graphene facilitate the transfer of electrons.

Keyword: Graphene, Dye-sensitized solar cell, Photoanode, Electrical conductivity

1. Introduction

Dye-sensitized solar cells (DSSCs) have attracted both academic and industrial interests as promising low-cost solar cells because of their relatively high photo-to-electric conversion efficiencies, low production cost, and environmental benignity since they were first reported on in 1991 by Gratzel *et al* [1]. The overall light- to-electric energy conversion yield claimed at that time was 7.1–7.9% in simulated solar light and 11% in diffuse daylight.

DSSCs use specialized materials for specific cell functions such as photon absorption, charge transport, and charge transport [2]. Figure 1 describe a simple energy diagram of how these devices function. A photon enters the solar cell through a transparent electrode and can be absorbed by a sensitizer, exciting an electron (a), as shown in Figure 1A. Then this electron can be injected into the conduction band of a neighboring semiconductor (b) and diffuse to the current collector (c). The electron can operate work and flow to the

*Corresponding author: *Won-Chun Oh*

cathode (d) where it is transferred to an electrolyte or a hole conductor (e). This material can then transfer an electron to the sensitizer (f), regenerating it and completing the circuit. To optimize these devices and accomplish respectable power conversion efficiencies (η, defined as the ratio of power incident on the solar cell to the maximum power produced by the solar cell). researchers have looked at ways to (i) maximize light harvesting and (ii) minimize losses due to parasitic electron transfer pathways (v, w, x, y, and z in Figure 1B) while also minimizing the over potentials required to drive the electron transfer in the desired direction (colored bands in Figure 1B).

Toward these ends, the archetypical DSSC (Figure 2) uses a fluorine-doped tin oxide (FTO) a transparent electrode commonly used as scaffold in solar cell with organometallic dye molecules as the photoanode, an iodide/triiodide redox couple dissolved in acetonitrile as the electrolyte, and a platinized FTO cathode [3]. Commercially, FTO commercially has a sheet resistance (Rsh) of ~15 ©/sq and transmittance of about 85% in visible light. FTO has a high resistance to corrosion associated with iodo species based electrolytes. TiO_2 nanoparticles provide a high surface area film (~ 1000×roughness for 10 μm thick) for increased dye loading [4], while sintering assures high connectivity of the particles for fast electron transfer and mechanical stability. DSSC dyes absorb light strongly in the visible range, they have extended excited state lifetimes, and their binding to the titania scaffold improves stability and charge transport. For instance, a ruthenium bipyridyl dye, N719, absorbs light with wavelengths up to ~ 800 nm, has an extinction coefficient of ~ 1.5×10^4 $M^{-1} \cdot cm^{-1}$ (at 535 nm), and has carboxylic acid groups that facilitate chemisorption to the titania scaffold [5]. To achieve efficient dye regeneration and charge carrier transport in DSSCs, a liquid electrolyte with an appropriate redox couple has often been used. Acetonitrile has been the solvent of choice for high-efficiency cells due to its low viscosity (0.34 mPa·s at 25 °C), facilitating ion transport, and its high electrochemical stability. The iodide/triiodide redox mediator was used in the original DSSC and had an unmatched efficiency until 2012, when a record DSSC (η = 12.3%) using a cobalt based mediator was reported [6]. In a simplistic view of this system, iodide regenerates the dye forming triiodide. Triiodide then diffuses to the cathode and is reduced back to iodide, which in turn can diffuse back to the photoanode and continue the cycle [7].

In order to improve the photovoltaic performance and lower the cost of DSSCs, incorporation of new materials has been considered. For instance, organic dyes have been synthesized and applied to replace the rare metal-containing dyes [8]. Additionally, both solid-state hole conductors and ionic liquids which have negligible vapor pressure and high ionic conductivities have been explored to replace the traditional organic electrolytes. At the cathode, transition metal compounds, conducting polymers, and carbon materials have been introduced as alternative catalysts to platinum in the cathode [9].

Graphene is a two-dimensional one-atom thick material that exhibits high thermal conductivity at room temperature (~5×10^3 W m^{-1} K^{-1}), high carrier mobility (2×10^5 cm^{-2} V^{-1} s^{-1} at an electron density of 4×10^9 cm^{-2}), high specific surface area (2600 m^{-2} g^{-1}) and high optical transparency (97.7%) [10]. All these advantages allow graphene to be a promising material for efficient and practical DSSCs. Graphene materials, with their

excellent electrical, optical, and mechanical properties, have been incorporated into each aspect of a DSSC (Figure 3). They were first used as transparent electrodes in 2008 [11] to replace fluorine doped tin oxide (FTO) at the photoanode and have since been used, for example, with the purpose of harvesting light, improving transport through both the titania layer and the electrolyte, and superseding platinum at the cathode. The unique properties and general applications of graphene materials have been reviewed by Neto, Geim [12] and more recently by Xu [13]. This review focuses on recent applications of graphene materials in photoanode, electrolyte and cathode sections of DSSCs, as will be discussed in this review.

The advantages of dye-sensitized solar cells paved the way for intensive research interest, which had reflected a tremendous increase in the number of publications in the past decade. A simple ISI Web of Knowledge search shows the rapid increase in the number of publications per year from literature search using the keywords "graphene", "DSSCs", and graphene in DSSCs (Fig. 4) [15]. Though the seminal work on dye-sensitized solar cells (DSSCs) was initiated in 1991 by Grätzel [16], the research has advanced at a rapid pace and a considerable amount of work has been made to improve the device efficiency from 7.1% in 1991 to 13% in 2014 [17], a level deemed as necessary for commercial and academic use.

Herein, we provide a comprehensive review of the use of graphene materials in DSSCs up through 2015 [18], inclusive, and critically evaluate the goals of using the material in each aspect of a DSSC, highlighting the major discrepancies which need further research for clarification. The interested readers could also refer to our previous review on fundamental concepts and novel materials used in DSSCs including panchromatic dyes, semiconductor photoanode, counter electrode, and electrolyte development for a complete understanding of the processes and parameters controlling their photovoltaic operation. By doing so, we aim to build upon the literature to suggest ways to not only to engineer better devices but also to define research goals for further developments. We begin by introducing graphene and the fabrication methods to produce the material as well as other related graphene-like materials. Then, we discuss the properties of these materials and their use in each area of a DSSC.

2. Synthesis Graphene Materials

Synthesis of graphene refers to any process for fabricating or extraction graphene, depending on the desired size, purity and efflorescence of the specific product. Since graphene's discovery in 2004 [20], many feasible, reliable, and versatile routes have been developed to prepare various kinds of graphene-based nanomaterials. This simple, low-cost technique has been widely used for the attention growth of interest in graphene [21]. Graphene flakes have been invaluable to the study and explanation of graphene properties. However, they are usually available at a size of several microns, have irregular shapes, and their azimuthal orientation is not deterministically controlled. Technological applications that take advantage of graphene's extraordinary electronic transport properties require structurally coherent graphene on a large scale, or large arrays of graphene flakes positioned with a unique azimuthal orientation on a substrate [22]. The

latter structures have not yet been demonstrated with flakes and this technology is expected to have limited relevance to commercial high-end electronic applications.

However, currently there are no standard criteria to evaluate graphene materials with, and information provided by authors is understandably incomplete. Thus, in this review we seek to give readers a sense of what the structure and properties of the graphene materials used are by providing basic information on the fabrication technique, with the idea that materials produced in similar ways will have similar structural features and properties [23]. A comprehensive description of graphene materials' production techniques and properties is not provided as they can be found in various recent publications. In addition, we summarize the synthesis methods, and comment on their maturity, advantages and disadvantages, and targeted applications.

Since graphene's discovery in 2004 [24], many reliable, feasible, and versatile routes have been developed to prepare various kinds of graphene-based nanomaterials, which can be categorized roughly into top-down and bottom-up methods. This session covers the graphene-based catalytic materials synthesis methods including micromechanical cleavage, exfoliation of graphite oxide (top-down), chemical vapor deposition (CVD), and other novel bottom-up methods. An overview of graphene synthesis techniques is shown in the flow chart in Figure 5 [25].

2.1. Top-down graphene

2.1.1. Mechanical exfoliation

Mechanical exfoliation (also known as "Scotch- tape method") is may be the eminent process for extracting single layer graphene (SLG) flakes on preferred substrates. The process of exfoliation is to divide the bulk of the layered materials into mono- or few-layer flakes by overcoming the strong van der Waals attractions between adjacent layers. The interlayer distance and interlayer bond energy is 3.34 A and 2 eV/nm^2, respectively. For mechanical exfoliation, an external mechanical force (300 $nN/\mu m^2$) is applied to decrease the potential energy between the interlayers [26], which It is mechanical exfoliation method that gave birth to graphene and was then extended to other related 2D materials such as transitional metal dichalco- genides (TMDs) [27], hexagonal-boron nitride (h-BN) [28] and etc.

At first, highly-oriented pyrolytic graphite (HOPG) was etched in oxygen plasma to get 5 mm-deep mesas on the top. Then, the mesas were pressed against a fresh wet photoresist on a substrate. After that, scotch-tape was used to directly peel flakes of graphite off the HOPG mesas [29]. Then the photoresist left in flakes were released in acetone after the peeling operation. Finally, mono- and few-layer graphene was produced by capturing the thin flakes with a specific substrate. After the mechanical exfoliation of graphene, micromechanical cleavage was then used to isolate individual crystal planes of related 2D materials [30].

It is by far the cheapest method to produce graphene. Graphene flakes obtained by mechanical exfoliation methods are usually characterized by optical microscopy, Raman

spectroscopy and AFM. AFM analysis is carried out on exfoliated graphene to assess its thickness and number of layers [31]. The single layers were obtained by repeated peeling of small mesas of highly oriented pyrolytic graphite with tape Figure 6. Though this approach was suggested to be highly reliable and allowed one to prepare a large area (up to 10 ¼m in size) of few-layer graphene (FLG, less than five layers including SLG) films, it is obviously not very efficient and thus was not widely used later except in the study of field effect transistor (FET) after its invention in 2004 [32]. Optical microscopy is another popular method of identifying single layer graphene. Depending on thickness graphene flakes give a characteristic color contrast on a thermally grown SiO_2 layer of 300 nm thickness on top of Si wafers [33]. In addition, Raman spectroscopy is also carried out on graphene acquiring by mechanical exfoliation. It is the quickest and most precise method of identifying the thickness of graphene flakes and estimating its crystalline quality [34]. This is because graphene exhibits characteristic Raman spectra based on number of layers present. Actually it is not easy to obtain larger amounts of graphene by this exfoliation method, not even taking into account the lack of sustainable flakes [35]. The difficulty of this method is really low, nevertheless the graphene flakes require to be found on the substrate surface, which is labor exhaustive. The quality of the prepared graphene is very high with almost no defects. The graphene formed by these mechanical exfoliation methods was used for production of FET devices (Fig. 6). Still, the mechanical exfoliation method needs to be enhanced further for large-scale, defect-free, high-purity graphene for mass production in the field of nanotechnology [37].

2.1.2. Chemical exfoliation

Chemical method is one of the best appropriate method for synthesis of graphene. In chemical method producing colloidal suspension which modify graphene from graphite and graphite intercalation compound. Different types of paper like material [38], polymer composites [39-41], energy storage materials [42] and transparent conductive electrodes [43] have already used chemical method for production of graphene. In 1860 graphene oxide was first manufactured Brodie [44], Hummers [45] and Stauden- maier [46] methods. Chemical exfoliation is a two-step process. At first reduces the interlayer van der Waals forces to increase the interlayer spacing. Thus it forms graphene- intercalated compounds (GICs) [47]. Then it exfoliates graphene with single to few layers by rapid heating or sonication. For single-layer graphene oxide (SGO) uses ultrasonication [48–52] and various layer thickness using Density Gradient Ultracentrifugation [53, 54]. Graphene oxide (GO) is readily prepared by the Hummers method involving the oxidation of graphite with strong oxidizing agents such as $KMnO_4$ and $NaNO_3$ in H_2SO_4/ H_3PO_4 [55, 56]. Ultrasonication in a DMF/water (9: 1) (dimethyl formamide) mixture used and produced single layer graphene. For this reason, interlayer spacing increases from 3.7 to 9.5 A . For oxidization high density of functional groups, and reduction needs to be carried out to obtain graphene-like properties. Single layer graphene sheets are dispersed by chemical reduction with hydrazine monohydrate [57, 58]. Polycyclic aromatic hydrocarbons (PAHs) [59–61], has used for synthesis of graphene. Using a dendrict precursor transformed by cyclodehydrogenation and planarization [62]. Produce small domains of graphene. Poly-

dispersed hyper branched polyphenylene, precursor give larger flakes [63]. The first were synthesized through oxidative cyclodehydrogenation with $FeCl_3$ [64]. Variety of solvents are used to disperse graphene in perfluorinated aromatic solvents [65], orthodichloro benzene [66], and even in low-boiling solvents such as chloroform and iso- propanol [67, 68]. Electrostatic force of attraction between HOPG and the Si substrate use in graphene on SiO_2/Si substrates [69]. Laser exfoliation of HOPG has also been used to prepare FG, using a pulsed neodymium-doped yttrium aluminum garnet (Nd: YAG) laser [52, 70]. Thermal exfoliation and reduction of graphite oxide also produce good-quality graphene, generally referred to as reduced graphene oxide (RGO).

2.1.3. Reduction graphene oxide

Chemical reduction of graphite oxide is one of the con- ventional procedures to prepare graphene in large quantities [71]. Graphite oxide (GO) is usually synthesized through the oxidation of graphite using oxidants including concentrated sulfuric acid, nitric acid and potassium permanganate based on Brodie method [72], Staudenmaier method [73], Hummers method [74]. Another approach to the production of graphene is sonication and reduction of graphene oxide (GO). Addition of H_2 occurs across the alkenes, coupled with the extrusion of nitrogen gas, large excess of $NaBH_4$ have been used as a reducing agent [75]. Other reducing agents used include phenyl hydrazine [76], hydroxylamine [77], glucose, [78] ascorbic acid [79], hydroquinone [80], alkaline solutions [81], and pyrrole [82]. GO was formed by the chemical reaction between organic isocyanates and the hydroxyl is shown in Fig. 7 also mention the FT-IR spectra of GO.

Electrochemical reduction is another means to synthesize graphene in large scale [83–85]. In 1962, first established monolayer flakes of reduced graphene oxide. The graphite oxide solution can then be sonicated in order to form GO nanoplatelets. The oxygen groups can then be removed by using a hydrazine reducing agent, but the reduction process was found to be incomplete, leaving some oxygen remaining. GO is useful because its individual layers are hydrophilic, in contrast to graphite. GO is suspended in water by sonication [86, 87] then deposited on to surfaces by spin coating or filtration to make single- or double-layer graphene oxide. Graphene films are then made by reducing the graphene oxide either thermally or chemically [87] a simple one-step, solvo thermal reduction method to produce reduced graphene oxide dispersion in organic solvent [88]. The colloidal suspensions of chemically modified graphene (CMG) ornamented with small organic molecules [89]. Graphene functionalization with poly (m-phenylenevinylene-co-2, 5-dioctoxy-p-phenylene- vinylene) (PmPV) [90], 1,2-distearoyl-sn-glycero-3-phosphoethanolamine-N [methoxy (polyethyleneglycol)- 5000] (DSPE-mPEG) [91], poly (tert-butyl acrylate). Here two cross-sectional FE-SEM and TEM pictures are shown in Fig. 8 for distinguishing GO and RGO.

2.2.1. Chemical vapor deposition (CVD)

One of the most developed methods to obtain higher yields of graphene-based nanomaterials is the graphite oxide exfoliation followed by post-treatment with

catalytically active species under varying reduction approaches. It is considered as the most feasible method within the top-down family for the production of graphene material in the industrial scale, because its raw material is naturally abundant low-cost graphite, and has much higher production yield as compared to micromechanical cleavage top-down or CVD bottom-up methods. In this CVD process a substrate is diffused on thermally disintegrated precursors in high temperature. It deposits on thin films, crystalline, solid, liquid or gaseous precursors on the surface of the substrate. The deposition of high-quality graphene from CVD process is usually done onto various transition-metal substrates like as Ni [92] Pd [93], Ru [94], Ir [95], and Cu [96]. CVD growth of graphene has been mainly practiced on copper [97, 98] and nickel [99- 101] substrates.

Graphene growth on copper shows that it may emerge as alternate route towards scalable growth of graphene with higher monolayer coverage [17, 73]. In 2009, the first CVD growth of uniform as well as large area graphene on a metal surface was done on polycrystalline Cu foils by exploiting thermal catalytic decomposition of methane [17]. Copper foil was an even superior substrate for growing single layer graphene films [17]. Although copper is an inexpensive substitute in contrast to other metals that is also simply extractable by etchants without chemically affecting graphene. For a very small solubility of carbon in copper, the carbon deposition process was found to be largely self-limiting [17]. The solubility of carbon in copper is negligible of the perspective of ppm even at 1000 °C [102] so the carbon precursor forms graphene directly on copper surface through growth step [17]. Cu surface is fully enclosed with graphene, save around 5 % of the comprising of BLG and 3LG [17, 102] area (Fig. 9). Surface roughness is known to produce graphene thickness variation on copper [103, 104]. Since graphene growth on copper is surface limited, so smoothness of copper surface imparts very significant role in receiving monolayer coverage across the whole surface of the substrate. Figure 7.

Due to few disturbing properties of Cu like surface roughening and sublimation; the researcher had to search for new substrates that was Ni substituting the Cu. Graphene was synthesized by Ni foil, polycrystalline nickel thin film, patterned Ni thin film The foils were first annealed in hydrogen and then bare to a CH_4–Ar–H_2 environment at atmospheric pressure for 20 min at a temperature of 1000 °C [105].The thickness of the graphene layers was found to be reliant on the cooling rate, with few layer graphene. Faster cooling rates conse- quence in thicker graphite layers, whereas slower cooling avoids carbon from separating to the surface of the Ni foil [105]. Still, the T range within which graphene can be grown on Ni is very thin, 100 °C [106], and could end in a Ni_2C phase [107], which can give rise to defects within the Ni crystal. In a nutshell any graphene grown on the surface could be non-uniform through the Ni–Ni_2C regions (Fig. 8). The problems of Ni synthesis were time-consuming exposure to the carbon precursor, not self-limiting, catalyzed growth with large number of wrinkles and folds.

Others method

There are several other ways to produce graphene such as electron beam irradiation of PMMA nanofibres [108], arc discharge of graphite [109], thermal fusion of PAHs [110],

and conversion of nano diamond [111]. Graphene can synthesis by arc discharge method in the presence of H_2 atmosphere with two to three layers having flake size of 100–200 nm [108, 112]. By rapid heating process Arc discharge in an air atmosphere resulted in graphene nano sheets that are 100–200 nm wide predominantly with two layers [113]. The conditions that are favorable for obtaining graphene in the inner walls are high current (above 100 A), high voltage (50 V), and high pressure of hydrogen (above 200 Torr). The vintage of graphene layer depends strongly on the initial air pressure [114]. He and NH_3 atmosphere are also used as arc discharge method [43]. In He atmosphere has considered gas pressure and currents to obtain different number of graphene sheets. In molecular beam deposition technique used ethylene gas source which deposited on a nickel substrate. Large-area, high-quality graphene layers were produced dependent on cooling rate.

3. Photoanode

The photoanode of a DSSC is made up of a semiconducting layer sensitized by a dye on a conducting substrate. The following three sections focus on the use of graphene materials as transparent conductors (section 3.1), in the semiconducting layer (section 3.2), and as the sensitizer itself (section 3.3).

3.1. Transparent Electrode

Transparent conducting films (TCFs) are required in traditional DSSCs as well as a host of other applications including flat panel displays and touchscreens. Due to this fact, TCFs are often studied independent of a particular device with the primary goal of minimizing RSh while maximizing transparency (particularly over the visible spectrum). Depending on the desired application, secondary goals can include flexibility, mechanical stability, chemical stability, and catalytic activity. Indium tin oxide (ITO) is the industry standard TCF, and it can boast RSh of 5 Ω/sq at ~ 90% transmittance (T) in the visible spectrum (often reported at 550 nm) [114]. Nevertheless, indium is a rare-earth metal, and ITO films are mechanically brittle, not compatible with strong acids, and not stable at high temperatures. FTO, an alternative TCF, is most often used in DSSCs as it is more robust to harsh chemical and thermal treatments (up to ~ 700 °C) which occur during solar cell fabrication [115]. Although cheaper than ITO, FTO films have higher resistivity per optical absorption, 15 Ω/sq at T ~ 85% [114]. Detailed reviews on traditional transparent electrodes can be found by Chopra *et al.* and Gordon [113,114]. To overcome cost and performance limitations of the transparent conducting oxides and to meet the drive for flexible electronics, there has been a strong push to develop alternative TCFs in both academia and industry. Due to the high electron mobility and transparency of single-sheet pristine graphene, graphene materials have been targeted as strong candidates to replace the conductive oxides. Overviews of the major advances and approaches have been recently reviewed in several publications [51,115–117]. As will be described in this section, although pristine graphene is unlikely to meet industrial targets for high- performing devices, electronically doped graphene materials and graphene"metal hybrid materials have already shown strong promise as transparent electrodes. We provide a synopsis of the

major fabrication techniques and performance milestones, starting with approaches using only graphene materials as TCFs and then follow up on this with hybrid material approaches. Lastly, specific uses of TCFs in DSSCs are reviewed.

Each layer of graphene absorbs about 2.3% of light; thus, for 90% transmittance, light can pass through a maximum of ~ 5 sheets [51]. Single-sheet measurements show that TRGO sheets with C/O above 300 (i.e., highly reduced material) have RSh of ~ 7.7 kW/sq (Figure 9B),67 while that for pristine graphene is ~ 6.45 kW/sq,66 suggesting that layers of the material can only achieve RSh around 1 kW/sq for T = 90%, even before accounting for contact resistances between individual sheets. In 2008, Wang *et al.* were the first to report on using a graphene material as a TCF, and they used the film as the window electrode (the electrode through which light enters) in a DSSC [26]. These TRGO films were formed by sequential dip coating of graphene oxide onto silica glass and then annealing the films at 1100 °C. High-temperature processing was required in order to reduce the material sufficiently, increasing the size of sp^2-hybridized aromatic networks (i.e., LA) and increasing conductivity as described in section 2. Those characterized for use as DSSC window electrodes were about 10 nm thick and had RSh = 1.8 kW/sq and T = ~ 62% at 550 nm. Although far from the performance achieved with FTO and lower than could be expected from single-sheet measurements, these cells demonstrated the proof of concept for the use of graphene materials as a transparent conductor and inspired many studies to advance this work. For instance, Becerril et al. spin coated thin layers of graphene oxide onto silica glass and reduced the films through different methods including hydrazine treatment and thermal annealing at 1100 °C [118]. They found that thermal annealing resulted in films which were over an order of magnitude less resistive than chemically reduced films at a given transparency, a result likely due to the higher degree of reduction achievable with thermal processing. However, their TRGO films still had an RSh of ~ 1 kW/sq at T = 80%. Zheng *et al.* were able to improve significantly on these results by creating large area graphene oxide (up to ~ 200 ¼m diameter sheets) and forming thin films through a Langmuir"Blodgett trough approach [119]. Large sheets are beneficial in reducing the number of boundaries and thus contact resistance of the tiled mosaic film, bringing the TCF closer to what could be achieved by a continuous graphene sheet. After high-temperature annealing, an R_{Sh} of ~ 600 Ω/sq was obtained at T = 90%, a value better than would be expected from the single-sheet measurements, but still almost 2 orders of magnitude higher than achievable with ITO.

De and Coleman analyzed over 20 studies of graphene material-based transparent electrodes and suggested a way to standardize the comparison of the various techniques [115]. This method relates the conductivity and transmittance of the material through the ratio of the dc conductivity (σ_{DC}) to the optical conductivity (σ_{Op}). The ratio can be then related to electrode properties through $T = (1 + ((z_0/(2R_{Sh})))((\sigma_{Op})/(\sigma_{DC}))-2$, where Z0 is the impedance of free space (377 Ohm). Their analysis showed that RGO (they term flakes) are severely limited by contact resistance between sheets (σ_{DC}/σ_{Op} limit of 0.7), with larger sheets (such as achieved the Zheng *et al.* approach or by CVD methods) achieving higher conductivity due to fewer contact regions. For reference, to achieve a 100 Ω/sq film at

T = 90%, σ_{DC}/σ_{Op} must be 35 or greater. Through their calculations, CVD-derived graphene is more suitable than a mosaic of sheets (σ_{DC}/σ_{Op} limit of 2.6), but it is still far from meeting commercial needs.

Nevertheless, De and Coleman note that conductivity limits can be greatly increased by increasing the carrier concentration through substrate interactions or electronic doping [115], an idea which follows from the fact that conductivity is equal to the product of a material's electron mobility, its charge carrier density, and the elementary charge. As previously discussed in section 2, electron mobility is correlated to the size of the aromatic domains, with highest values obtained for pristine graphene. Yet, the charge carrier density of pristine graphene is low, resulting in an R_{Sh} similar to that of the RGO material.66 Thus, in order to meet the performance of conventional TCFs, increasing the charge carrier density of the graphene materials is necessary. Electronic doping can occur through incorporation of electron-donating or -accepting species into the graphene lattice or more commonly through adsorption of these species on sheets. Both HNO_3 and $SOCl_2$ are common examples of chemicals used for the latter electronic doping method. By electronic doping, Zheng et al. decreased R_{Sh} in their TRGO films almost 25% to 459 Ω/sq at T = 90%, a significant improvement but still over an order of magnitude more resistive than ITO films.116 Bae *et al.* were able to create industrially relevant TCFs by stacking four monolayers of CVD–graphene and then electronically doping the film with HNO3.120 These films, which measured 30 in. (0.76 m) along the diagonal, exhibited an RSh ≈ 30 Ω/sq at T = 90%. Further improvements to mobility or charge carrier concentration could further decrease the resistance.

Alternative approaches to achieve high performance have included forming hybrid materials. For instance, both [CVD- derived graphene]–CNT [120], and CRGO"CNT [121] hybrid films have been produced, as have CRGO"[silver nanoparticle] hybrid films [122]. The best performance to date of graphene- based TCFs has been with [CVD-derived graphene]–[metal nanowire] films. Through photolithography, Zhu *et al.* created metal nanogrids (Au, Cu, and Al) with grid lines 100 nm thick and 5-10 ¼m wide, spaced 100-200 μm apart [123]. CVD- derived graphene was then used to coat the grid and form a continuous conductive network. In this case, the relatively thick metal grids act as the primary current collector reducing the need for graphene materials with super high mobility and charge carrier density. Using grid boxes smaller than the grain size of the CVD-derived graphene, which has been shown to be dependent on the grain size of the metal substrate, i.e., copper, potential high-resistance zones can be avoided. As charge is supposed to be transferred from the graphene material (which covers much more of the surface than the metal) to the metal grid the contact resistance between these materials becomes important with this system. Nevertheless, these hybrids have reachedR_{Sh} of ~ 3Ω/sqat T = 80%or ~ 20Ω/sqat T= 90% [124]. Figure 10 provides an overview of what has been achieved for graphene-based TCFs. Even though Wang et al. first reported graphene as a DSSC window electrode, further reports in this application have been scarce. Bi *et al.* demonstrated the growth of CVD-derived graphene directly on silica glass substrates and used these as the current collector at the cathode of a DSSC (light entered

the cell through the anode) [125]. However, the devices were hindered due to the relatively high R_{Sh} compared to FTO (1449 Ω/sq at T = 79.5% and 63 Ω/sq for opaque films). Both Cottineau *et al.* and Wu *et al.* studied how to electrodeposit metal oxides onto mechanically exfoliated graphene and CRGO, respectively [126,127]. Although these films were not employed in a solar cell, the approaches developed represent a first step toward creating thin film, flexible photocathodes for DSSCs.

As researchers have fabricated graphene-based transparent electrodes with R_{Sh} < 30 Ω/sq at T = 90%, approaching the performance of conventional FTO and ITO electrodes, it is evident that graphene electrodes can enter the market. However, it is not clear if they will do so and if so when. The scalability of the technology and cost reductions must be demonstrated to be used in commercial devices. With regard to DSSCs, extra constraints may arise depending on the electrolyte and solar cell design. For instance, metal hybrid electrodes would likely corrode in an iodine-containing electrolyte. In any case using graphene materials in transparent electrodes is far from mature, and more advances will be made, particularly for applications in which the current TCFs do not work well, such as low-temperature substrates and flexible devices.

3.2. Semiconducting Layer

In a DSSC, a photoexcited electron is injected from the dye into the semiconductor where it diffuses to the current collector. Losses occur for several reasons including due to the voltage drop between the dye LUMO level and the Fermi level of the semiconductor, from the ohmic resistance in the semiconducting layer, and from recombination of injected electrons with the dye or with oxidized species of the redox couple. In this last case, electrons from the semiconductor or from the current collector (i.e., FTO) can recombine with the electrolyte. Many techniques have been developed to minimize these losses. For instance, anatase phase TiO_2 energy levels match favorably with many dyes, providing injection efficiencies near unity, [128-130] with acceptable voltage drop. Moreover, it has been shown that TiO_2 has a low recombination rate with triiodide (of the common iodide/triiodide redox mediator); thus, dense layers of TiO_2, ~ 20-100 nm thick, are often used as a blocking layer to prevent recombination from FTO to triiodide. [131-133] Lastly, TiO_2 has a relatively high conductivity for a semiconductor due in part to oxygen vacancy n-doping and photoexcitation of electrons in the material. It has been shown that crack-free, sintered films optimized for DSSCs can exhibit electron diffusion lengths significantly longer than the film thickness itself, resulting in near unity charge collection efficiencies [134-136]. The film thickness (generally 10-20 μm) is chosen in order to have adequate light harvesting and is determined by the surface area of the semiconducting scaffold and the extinction coefficient of the dye.

Although best practices are widely disseminated, only a few laboratories have been able to create DSSCs with efficiencies of over 10%, providing a testament to the difficulty in replicating these best-in-class devices. Thus, as an alternative approach, many groups have sought to use graphene materials to improve the performance of the semiconducting layer in DSSCs. Below, we first describe the use of graphene materials in the blocking

layer to prevent recombination between the FTO and triiodide. Then we discuss the use of graphene materials in the TiO_2 scaffolding to improve photocurrent density and explore the rationales provided (e.g., improved electron transport, dye adsorption, and light scattering) for the observed improvements. We reiterate that best-in-class devices have overcome many of the limitations arising from FTO recombination and TiO_2 charge transport without using graphene materials; however, we cannot rule out that the techniques described in this section could provide a more commercially feasible way of achieving similar results.

To our knowledge, the first use of a graphene material in the semiconducting layer of a DSSC was reported by Kim et al., who used a photocatalytically reduced graphene oxide –TiO_2 nanoparticle composite (TiO2 particle diameter < 10 nm) as a blocking layer with the idea that the flat sheets could be deposited at low temperatures and without dangerous chemicals, unlike the common $TiCl_4$ treatment, and that they would provide a barrier between triiodide and FTO [137]. The group demonstrated a 7.6% relative improvement in efficiency over a cell without a blocking layer. However, due to significant light absorption from the film (T decreased from 85% to 78%) and potential catalysis of triiodide reduction (see section 5), their approach does not seem to be more beneficial than the traditional TiO2 blocking layers. Several other studies used similar approaches [29,34,138] and also saw improvements. For instance, Chen *et al.* spin coated thin layers of TRGO as a blocking layer, resulting in an 8.1% efficient cell, which was better than a cell without a blocking layer (η = 7.2%) and better than one with their $TiCl_4$ pretreatment blocking layer (η = 7.5%). The improvement was due to an increase in photo- current [29]. Interestingly, the blocking layer only absorbed 1.6% of light, suggesting that, on average, less than a monolayer of TRGO was present or that the TRGO was only slightly reduced, resulting in a less absorbing material. Graphene oxide would provide a barrier for electron recombination with the FTO, but it would also provide an insulating barrier, so only very thin layers which allowed tunneling could be effective. Furthermore, graphene materials can only work effectively for a blocking layer if they are less active for the redox mediator than FTO is. Although this is likely the case with the triiodide mediator, and hence the improvement reported, it is not universally the case (for instance, graphene materials are highly active for the Co(bpy)3(II/III) couple, where bpy is bipyridine, see section 5).

A more established use of graphene materials has been their incorporation into the semiconducting layer itself [28,29,31-34,138]. A driving motivation for this work was to increase device performance through increasing charge collection efficiency, i.e., photocurrent, in the photoanode. A typical DSSC has a 10"20 ¼m thick layer of TiO_2. Thus, electrons photogenerated in the rear of the device have to diffuse to the front to be collected, a length on the order of 100 ¼m assuming a random walk. The collection efficiency as a function of electron diffusion length and film thickness can be approximated by examining electron transport and electron recombination time scales as shown in Figure 11.

One method to increase collection efficiency is to improve electron transport in the TiO_2 (i.e., increase the diffusion length), as is done with the sintering process. An alternative

method is to decrease the electron path distance, which can be done by creating finger electrodes into the TiO_2 layer as reported by Chappel et al. and later by Joanni *et al.* [139-141] A schematic of the approach can be seen in Figure 12. In these studies, the approach was significantly limited by the primary particle size of tin oxide or ITO used in the electrode material as well as by the need to coat the conducting fingers with a blocking layer of TiO_2 (at least 6 nm) to prevent recombination in the device [142]. Graphene materials hold a distinct advantage here due to their atomic thinness and high aspect ratio which provide a low percolation threshold [143]. Ideally, they could act as a current collector with only slight changes to the TiO_2 film morphology. For best results, a conductive graphene material should be used which has minimal defects for catalytic activity (see section 5) or which can be effectively coated by a dense TiO_2 layer. As described below, several studies have used graphene materials to this effect, with between 0.5 and 1.0 wt % inclusion of the material providing the best results. Although some studies report increased TiO_2 conductivity as the primary cause for improvement, others claimed it was due to unforeseen side effects such as increased dye loading and light scattering in the electrode. The following section treats each of these effects in turn.

The first study on this topic was published in 2010, in which Yang *et al.* argue that graphene can act as an electron bridge in the photoanode, shuttling electrons to the current collector and lowering recombination in the device [28]. Unlike in the schematic above, there was no attempt to completely coat the conductor with the semiconductor. Nevertheless, in this work, they saw an increase in device efficiency from 5% to 7% by first adding 0.6 wt % CRGO into the TiO_2 particle film (commercial P25 particles) and then heating the composite to 450 °C to sinter the TiO_2 and further reduce the CRGO. The improvement was solely the result of increased photocurrent. Since then over a dozen studies reproduced this effect and tried to elucidate the improvement mechanism. Results from these studies are compared to control cells in Figure 13. In studies where several compositions were tested only the top performing case was included. The authors discussed several means of improvement to explain these results. At least five studies reported that adding graphene materials to the TiO_2 layer resulted in an increase in dye absorption, [32,139,141,142,144] which in turn increased the light- harvesting efficiency and accounted for an increase in photocurrent. However, other studies did not see a change in dye absorption, [28,33,138] and some reported a lower absorption, [29,140,145] even though all of these studies report a higher photocurrent.

The study by Yang *et al.* also reported that inclusion of RGO induced formation of macropores in the TiO_2 films which acted to scatter light [28]. The authors state that this effect could be responsible for up to 7% of the 39% increase in photocurrent observed. Fang et al. hypothesized that porosity was due to voids formed from the reduction in volume of graphene oxide during heating [146]. At elevated temperatures, graphene oxide becomes dehydrated and residual oxygen groups are removed. Although the width of RGO is about one-half that of graphene oxide, this change is on the nanometer scale and thus cannot be responsible for the reported light scattering, an effect that would require macroscopic porosity. An alternate explanation would be that including RGO in the system

affected the rheology of the paste (likely greatly increasing the viscosity), preventing smooth and dense film deposition. Furthermore, Durantini et al. found that a [solvothermally reduced graphene oxide]-TiO_2 composite absorbed 44% more light at the dye's (N719) absorption peaks (~370 and ~500 nm), which could explain the full increase in photocurrent in their study (29%). Although they attributed this result to light scattering, the authors also mentioned that they could not rule out other optical effects, such as the TRGO acting as a sensitizer itself. Besides direct sensitization (for more direct studies on this see section 3.3), enhanced light harvesting could be due to increased absorption in TiO_2. In photocatalysis studies, it has been shown that the presence of graphene materials can reduce the band gap of TiO_2 into the visible spectrum, speculatively through Ti-O-C bonding, [147,148] and Peining et al. report a 25 nm red shift in absorption for a TiO_2 film incorporating thermally annealed CTAB-functionalized graphene. Even more surprising is the report of the shifting of the TiO_2 band gap to 2.11 eV (588 nm) with inclusion of 1 wt% CRGO [149].

Increased dye absorption and scattering contribute to improved performance; nevertheless, based on electrochemical impedance spectroscopy (EIS) data, Yang et al. proposed that increased collection efficiency was primarily responsible for their observed increase in performance [28]. Many studies have looked into how to interpret EIS spectra for DSSCs [150-151]. EIS provides information on interface resistances (and capacitances) in electrochemical systems. For DSSCs, this can include the series resistance of transport through the current collector (RS), charge transfer resistance (RCT) at the cathode/ electrolyte interface, resistance between the TiO_2 particles (represented by a transmission line model), TiO_2/electrolyte recombination resistance (RR), and diffusion resistance (ZD). A simple resistor in parallel with a capacitor, such as is the case for the cathode/ electrolyte interface, is represented by an arc in a Nyquist plot, while the transmission line arises as a diagonal line at high frequencies. These features can be seen in Figure 14. It is important to note that the interpretation of EIS data is only as good as the equivalent circuit used, with the most widely used models shown in Figure 15 (Figure 14A is in the dark; Figure 14B is in the light, where TiO_2 becomes more conductive due to increased electron density). In addition to the magnitude of resistances, the characteristic frequency that a resistance is observed at can provide insight into electron transport. For instance, the electron lifetime, and from this the diffusion length, can be approximated from the characteristic frequency of the TiO_2/electrolyte interfacial resistance arc, where frequency is proportional to the inverse of the electron lifetime [152]. However, depending on the materials used and how the device is fabricated, spectra for various resistances may overlap in frequency and the interpretation is less clear without additional measurements. This overlap is especially important when evaluating the photoanode as the resistance between TiO_2 particles (transmission line) and the resistance of the TiO_2/electrolyte interface occur at similar frequencies and thus have an ambiguous interpretation [153,154]. Unfortunately, this ambiguity is often ignored in the publications, and it is aggravated by the fact that the resistance between TiO_2 particles should be minimized and TiO_2/electrolyte resistance should be maximized (shunt resistance) in high-performing DSSCs.

Yang *et al.* see two semicircles in their impedance spectra as displayed in a Nyquist plot.28 They assign the high-frequency semicircle to RCT, which is consistent with a large body of literature for using platinum counter electrodes (see section 5 for more details). They then claim that a lower resistance at midfrequencies represents improved electron transport in the film. The characteristic frequency of this arc is also shifted, which they interpret to be representative of the electron lifetime. Chen *et al.* made a similar analysis with 0.02 wt % CRGO incorporated into their TiO_2 film [29], as did at least 10 other studies. [31,33,138-145] However, another body of work sees an increase in the middle frequency semicircle upon inclusion of graphene materials, which they claim to be due to RR. Thus, for these works, the authors report that a larger resistance represents a decrease in electron recombination to the electrolyte and higher collection efficiency [32,34,146,147]. This interpretation is supported by the most extensive EIS studies for TiO_2 films. With appropriately sintered TiO_2, the resistance between TiO_2 particles is seen primarily in the dark, and RR dominates under illumination due to the photoconductivity of TiO_2. [34] In a detailed EIS study undertaken at various bias potentials and using a DSSC equivalent circuit developed by the Bisquert group, it was determined that the photocurrent improvement was not due to a reduction in recombination nor from a shift in the Fermi level. [34] Under light, the TiO_2 film conductivity was too high to measure, suggesting RR to be negligible, in agreement with previous studies on the photoconductivity of the TiO_2 layer [156-158]. With this interpretation, a decreased midfrequency semicircle could represent greater recombination, perhaps caused by graphene materials acting as recombination centers due to their activity toward triiodide reduction (see section 5). This recombination could be minimized by effectively coating the sheets, or networks of sheets, with TiO2 as was attempted for the FTO finger electrodes.

Some groups have used graphene materials for both of the roles discussed above, showing successive improvements. Chen et al. used CRGO in the blocking layer and in the TiO_2 scaffold layer [29], while Tang et al. incorporated CRGO in the blocking, scaffold, and scattering layer leading to a much more efficient device (η = 9.24% compared to 6.25% for a device with just a TiO_2 scaffold layer). In a relatively backward approach, Song et al. coated the top of the TiO_2 layer with CRGO (FTO– TiO_2–CRGO structure) and reported an improvement in photocurrent and efficiency over control samples as well [153], an improvement which is not adequately justified in the work and cannot be explained by the authors of this review. How these devices would compare to those optimized with current best practices for blocking, scaffold, and scattering layers is unknown, but it is clear that the performance increase, if any, would be greatly diminished.

Graphene materials have been incorporated into the semiconductor film in a variety of ways including grinding of powders [159], ball milling [147], colloidal aggregation [34], and coelectrospinning [32]. To prevent sheet aggregation, Park et al. claim to first coat Al_2O_3 with graphene oxide and then mix these coated particles in with TiO_2, where they are then heat treated. This approach requires a large fraction of inactive material (aluminum oxide) in the DSSC. Similarly, Li et al. saw improvements in DSSCs with a TRGO–YF_4: Er^{3+}/$Yb3^{+}$– composite mixed into TiO_2 [160], though it is unclear why this

system was chosen. Lastly, in addition to the traditional TiO_2– dye DSSCs described above, graphene materials have been incorporated into quantum dot photochemical cells [142,161] and in p-type DSSCs [162]. In the latter case, the conductive properties may play a much larger role due to the low conductivity of NiO which is used as the dye scaffold and hole conductor. In almost all approaches described, whether the initial material was graphene oxide, CRGO, or TRGO, the cells underwent sintering conditions at temperatures between 300 and 500 °C resulting in an RGO material. Because of this, as the paper by Wang *et al.* illustrates, it may not be necessary to start with RGO. Processing graphene oxide, which is readily water dispersible, rather than RGO, could simplify hybrid photoanode fabrication [33].

It is clear that graphene materials can play a variety of roles in the semiconducting layer of a DSSC photoanode and that addition of these materials can improve a poor or mediocre device's performance. Nonetheless, it is still unclear whether addition of graphene materials into best-in-class cells would have an improvement. In these optimized devices, TiO_2 blocking and scattering layers are effective at reducing recombination and increasing light harvesting, respectively. Furthermore, TiO_2 films can be fabricated without cracks, and they can be sintered to provide a highly photoconductive network. In these devices, electron diffusion lengths have been measured to be much larger than photoanode thicknesses and collection efficiencies near unity are reported. One study, by Neo and Ouyang, suggests that improvements may not be realized for cells which have undergone further optimization such as we have described. In their work, graphene oxide was used as an auxiliary binder and 13 μm thick crack-free films were able to be formed from a single doctor bladed layer, rather than the four layers typically required with commercial pastes [162]. The cells were then heat treated, sintering the TiO_2 and reducing the graphene oxide. In these devices, which employed TiO2 blocking and scattering layers, the performance of devices made with and without TRGO was nearly identical (η = 7.70% and 7.76%, respectively). In line with this work and the results presented above, it is the opinion of the authors of this review that incorporating graphene materials into the photoanode will not improve upon current best practices, though it could provide an alternative method of achieving the same goals.

3.3. Sensitizer

An effective sensitizer for a DSSC must be able to absorb a significant portion of the solar spectrum and be able to inject excited electrons into a semiconducting scaffold faster than they relax to the sensitizer's ground state. As previously mentioned, N719, one of the most prevalent dyes, absorbs wavelengths up to ~ 800 nm and has an extinction coefficient of ~ 1.5 × 104 $M^{-1} \cdot cm^{-1}$ (at 535 nm). It achieves near unity charge transfer into TiO_2 due to chemisorption of the dye's carboxylate groups onto the TiO_2 surface, facilitating electron injection. As reviewed in detail by Hagfeldt *et al.*, [3] researchers have synthesized thousands of dyes with the goal of increasing light harvesting and reducing recombination in the solar cell. Pristine graphene is known to have a broad and strong absorption profile, absorbing about 2.3% of light with each monolayer of material; [69] thus, it has received interest as a possible sensitizing material.

A few studies add credence to this possibility as they report that efficient charge injection from graphene materials to TiO_2 can occur and that graphene can act as a photosensitizer. However, graphene materials have shown poor performance to date in this role. Nevertheless, they have recently shown promise in hot injection [164] and multiple carrier generation, [165] providing a means to surpass the Shockley"Quiessar efficiency limit inherent to current device structures.

Long *et al.,* using nonadiabatic molecular dynamics formulated within the framework of time-domain density functional theory, showed that photogenerated electrons can be transferred from graphene to TiO_2 about 3-5 times faster than they would recombine in the material through relaxation.173 The ultrafast injection was due to electronic coupling between graphene and TiO_2, with the surface oxygen atoms of TiO_2 forming bridge structures to the graphene sheets. Similar results were obtained by Du et al. using density functional theory calculations to look at injection in the (110) surface of rutile TiO_2. Recently, Williams *et al.* determined that photoexcited graphene quantum dots (GQDs) inject electrons into TiO_2 with a time constant below 15 fs, suggesting that hot injection (wherein charge carriers are injected before being thermally equilibrated to the conduction or valence band) may be possible [166]. In addition to being able to transfer charge into TiO_2, Zhang *et al.* experimentally demonstrated that graphene materials (TRGO, hydrothermal method) can act as a photosensitizer [167]. This work discounted the possibility that TRGO only acted to narrow the band gap of the semi- conductor (see section 3.2 for further discussion of this).

Putting these ideas into practice, Yan *et al.* fabricated the first DSSC using graphene material photosensitizers. This device used GQDs which ranged from ~ 1 to 30 nm in diameter and had an absorption maximum at 591 nm and an extinction coefficient of 1.0 × 105 $M^{-1} \cdot cm^{-1}$, almost an order of magnitude higher than N719. Additionally, the HOMO level was determined to be below the iodide/triiodide redox potential, while the LUMO level was above the TiO_2 conduction band, suggesting that both electron injection and dye regeneration are possible, see Figure 16A. A later study by the same group showed that the GQD band gap can be tuned by controlling the size of the molecule and that the redox potential can be tuned by changing its functionalization. [168] Furthermore, they show that the effect can be predicted through tight-binding calculations and provide a route to design sensitizers with specific properties. Although important as proof of concept devices, DSSCs using GQDs recorded poor performance (η = 0.06%, Figure 16B) due primarily to very low photocurrents, which can be at least partially attributed to poor adsorption of the GQDs onto the TiO_2 [169]. Potentially addressing this issue, Hamilton et al. have shown that the orientation of GQDs can be controlled for monolayers by tuning the edge functionalization (Figure 16C) [170]. The group was able to achieve horizontal or edge alignment of the GQDs using a Langmuir–Blodgett trough setup. If this result could be made applicable to porous TiO_2 surfaces then light-harvesting problems seen in the earlier DSSC work could be reduced. In the case of edge-aligned GQDs, the charge transfer would have to be examined, as previous simulations assumed a horizontal alignment.

Although graphene materials can be used as a light absorber in DSSCs, the more the structure is optimized (smaller, specific functionalities, etc.) the more it appears to approach traditional organic dyes that have been synthesized. An as of yet unrealized advantage of graphene materials as sensitizers is the possible large-scale production of the product through top-down procedures such as the oxidation and reduction of carbon fibers, [171] nanographite, [172] CNTs, [173] or carbon black, rather than an expensive bottom-up synthesis currently employed for most dyes. Lastly, perhaps the largest role of graphene materials as a DSSC sensitizer would be in a scenario which took advantage of the quantum effects and allowed for ultrafast injection in order to overcome intrinsic limitations to conventional devices.

4. Electrolyte

To achieve efficient dye regeneration and charge carrier trans- port in DSSCs, a liquid electrolyte with an appropriate redox couple has often been used. To further improve the performance of the electrolyte requires that; (i) the electrolyte must be electrochemically stable over the potential range experienced in a DSSC, (ii) be transparent, (iii) have minimal potential losses due to the mismatch between the dye HOMO level and the electrolyte redox potential, and (iv) have fast charge transport, i.e., small redox species and low-viscosity solvent. For long-term stability, the electrolyte should be nonvolatile. Unfortunately, a solvent's viscosity and volatility are generally inversely related, complicating the development of commercial DSSC with high efficiencies. To address some of the limitations of electrolyte systems, graphene materials has been incorporated into the electrolyte of a DSSC [174]. The incorporation of graphene materials with electrolyte can be categorized undo two main reasons; as an additives and as the main constituent (>1 wt.%).

As an additive, graphene can be used to reduce the resistance of highly concentrated conductive fillers of an electrolyte in DSSC. Although significant improvement has not been achieved with graphene in the electrolyte, their application has shown to be well sui- ted as a minor component [174] used 0.005 wt.% of nano-ribbons graphene to reduce the optical absorption of iodide/triiodide electrolyte upon illumination. This was achieved through the transfer of electron from graphene nano-ribbon via triiodide to reduce the path length of the absorb- ing species. The iodide/triiodide electrolyte absorbs light energy between 350 nm and 400 nm spectral wavelength however; in DSSCs, its application was to generation photocurrent [175] in an inverted configuration where the device absorbs light energy via the electrolyte through to the photoanode. The inclusion of graphene nano-ribbons with the electrolyte has led to an increase in efficiency for inverted configuration from 5.8 to 7.0% and with conventional design, efficiency of 8.5% was achieved (Fig. 17) [174]. Contrarily, the use of graphene mate- rial in electrolyte led to the formation of gel in solvents based on ionic liquid [176] although this depends on the propor- tionality of the mixture.

Electrolytes containing graphene have shown to exhibit negligible reduction in the diffusion resistance with increases in the amount of graphene oxide. Studies supported

that electrolyte containing graphene oxide performs better (PCE = 7.5%) than liquid electrolyte without graphene (PCE = 6.9%) and was attributed to increase in the fill factor (Gun *et al.,* 2012). Although there was no outlined mechanism to check for long-term performance of the device, Neo and Ouyang [177] found that graphene oxide acts as a gelator for methoxypropionitrile which is known for its low-volatility. Further enhancement can be achieved by tuning the particle sizes of graphene oxide by using different sonication time. This is an effective approach because the particle sizes are inversely related to the ionic conductivity that are formed [177]. DSSCs incorporating thoroughly ultrasonicated graphene oxide retain high performance over a month of consistent testing and marginal reduction in PCE was observed as the day lengthens [174,178] Although much concern has been driven by the enhancement of device performance with the formation of gelation using graphene, formation of well-tailored ionic liquids could lead to a shift in concentration.

Graphene materials have shown to be a suitable material to enhance the effectiveness of charge transport in electrolyte [179]. However, the percolation of graphene should be regulated between the contact connecting to the anode and the cathode so as to avoid short circuit leading to drop in performance of the device. Graphene sheets with average particle size of 10 nm exhibits an effective charge transport and can be considered large to TiO2 pores. Graphene materials are to possess high sp2 hybridization in order to be conductive; therefore preference is given to TRGO or graphene extracted from exfoliated liquid and the solvent [180] because of their high absorption capability of visible spectral wavelength and their ability to pre- vent back illuminated light transfer. Range of solvents used for graphene is presented in Table 3.

Gell based electrolyte formed from a highly concentrated exfoliated graphene solution (30 wt.%) containing 1-methyl 3-propyl imidazolium iodide (PMII) improves the conductivity of electrolyte and device performance from 0.16 to 2.20% [181]. Nevertheless, attention has not been drawn specifically if the inclusion of PMII led to enhanced performance of the device, the improvement of the electrolyte conductivity or the shorter electrolyte diffusion length that facilitated the percolation of graphene material at the cathode to create a porous carbon counter electrode. In an attempt to improve the conductivity of the electrolyte, lower concentrated graphene oxide (6.5 wt.%) solution has been used to reduced 1-octyl-2,3-dimethylimidazolium iodide (ODI) and iodide based electrolyte using solvothermally process. The device performed better than those without TRGO and those based on acetonitrile (PCE = 5.8%, 3.6%, and 5.1%) [182].

It became evident that the inclusion of graphene material into the electrolyte was severely affected by the catalytic activities facilitated by the reduction of triiodide by graphene leading to the emergence of a short circuit device [183]. Therefore, graphene is compatible with device application as a component of the electrolyte as a minor additive specifically to reduce the absorption of energy in electrolyte. Therefore, graphene incorporation into the electrolytes for a high performance device is feasible in small proportion.

5. Counter electrode

Conventional sensitized solar cell based on organic dye incorporates redox mediators to facilitate charge transport as reduced species facilitate dye regeneration and the oxidized species are reduced at the cathode. Certain criterions that are in check to ensure that the system works efficiently encompasses firstly, the ability of the redox species to diffuse readily from the anode through to the cathode, secondly, the rate at which dye regenerates via the reduced species should be swifter than from the scaffold and thirdly, reduction rate exhibited by the redox species at the anode should be relatively slow but must be very fast at the cathode. Graphene materials have been used in a variety of ways to reduce electrolyte diffusion in redox species especially in the triiodide based electrolyte. Solar cell incorporating triiodide, Co(bpy)3 (III) requires lessen over-potential at the cathode to the over- potential and to reduce mediator species [184, 185]. Cathodes comprising of platinum deposited onto FTO have been used by many researchers because of their high activity with iodide/triiodide mediator [186-189]. Although their stability has not been known specifically with heavy metal in sensitized solar cell device [190-192].

Stability test of Dyesol Platinum as counter electrode has shown to be consistent in performance over 11,000 h [191] except that the material is expensive and requires high tem- perature exceeding 400 °C. Therefore, its application in solar cells is not considered as a cost-effective option for device fabrication. Graphite has found their usefulness in DSSC as counter electrodes since 1996 [192]. Research on graphene materials as cathode material has been intensified by its high surface area, high conductivity, tunability of the properties and cost- effectiveness [193]. Graphene materials have been subjected to modification as a replacement for platinum (Pt) with iodide/triiodide redox electrolyte and with other electrolyte like Co (bpy)3(II/III).

The quest for a Pt-free solar cell represent a shift towards exploring unique properties of low-cost counter electrode such as graphene-based materials for solar cell. Conducting polymer [194-196] and carbon-based materials [197-200] are among the materials that has been used as composite material with transition metals based inorganic materials to replace Pt as counter electrode. Pt-free materials based on carbon nanotubes (CNT) have been used as counter electrode in DSSCs to achieve over 10% efficiency [201]. However, flexible electrode to replace FTO glass using polyethylene naphthalate (PEN)/polyethylene terephthalate (PET) coated with a thin film of ITO have been used in DSSC [202]. The conductive coating was very sensitive to bend and expensive. Alternatively, carbon-enriched conductive textile materials has been explored as an ideal counter electrode in sensitized solar cell. Among the textile materials to prepare counter electrode include nylon [203], polyester [204] and cotton [205] and has been used in DSSC as flexible and low-cost carbon materials. Cotton material appears to have a better performance among other carbon-based materials.

Extremely conductive 2D graphene coated fabric (HC-GCF) based on cotton has been used as counter electrode in DSSC. The materials have shown to increase the spectral adsorption wave- length of graphene oxide thin film [206]. The surface charge was shown to be negative, which implies that the coating may not last as required. Alternatively,

surface charge of cotton- based fabric cheaper than Pt has been altered to form a self-assembled with high electrical conductivity and requires no high temperature treatment as in Pt. The counter electrode can be pre- pared using dip and dry technique and then subjected to chemical reduction [207]. With these innovative breakthroughs, graphene materials will in near future replace Pt as counter electrode to pave way for a low-cost, flexible and efficient cells DSSC.

6. Hybrid electrode

The competitive opportunities arising from the use of graphene materials as a cost effective material in solar cell to replace expensive platinum is ongoing. Study have shown that composites graphene material are effective conductive scaffold material and initiates high catalytic activity (Fig. 18).

Vertically aligned CNTs grown as standalone cathodes on a conductive substrate (Li *et al.*, 2011) of about 3 lm thick having RSh of 50 W/sq has shown to be 4 times better in performance than FTO. Composite CNT–CRGO film has a lower R_{Sh} and charge transfer resistance (RCT) (15 W/sq, 1.4 W) compare to CRGO (94 W/sq, 20 W) or CNT films (30 W/sq, 4.3 W) [208].

Electrophoretic deposition has been used to co-deposit CNTs and RGO based on microwave-assisted reduction (Zhu et al., 2011) the peak performance was found at 60% CNT, 40% RGO [209]. Hybridized graphene materials incorporating polymers improved conductivity and catalytic activity. TRGO films incorporating Nafion and polyvinylpyrrolidone binders have shown to have low-porosity TRGO films leading to low catalytic activity [210,211]. Graphene based materials have been used to improve the performance of platinized FTO electrodes, using platinum–RGO hybrid electrode [211-214]. However, a layer of CRGO formed between FTO and platinum can reduce platinum loading to 0.2 mg/cm^2 leaving performance close to the sputtered platinum (7.7–8.2%) [215]. Using photo-assisted co- reduction of chloroplatinic acid and graphene oxide, 3 nm particles of RGO formed onto FTO (1 mm thick) by spraying outperformed a platinum film formed through a low-temperature sputtering [216]. Alternate method to co-reduced graphene oxide and chloroplatinic acid using microwaves has been suggested [217]. Chartarrayawadee *et al.* (2012) reported that co- deposited CRGO and platinum is preferred to subsequently layer by layer from graphene sheets because of the tendency of low-permeability of diffusion to the underlying platinum layer.

Nanoparticles incorporating metallic materials deposited on RGO with $Ni_{12}P_5$ and MoS_2 has been reported [218-220]. An 8 nm diameter Ni particles deposited on TRGO using laser ablation outperformed similar material deposited by sputtering technique [221]. The activity of graphene formed by CVD was improved by depositing 30–50 nm diameter CoS particles sizes by successive ionic layer absorption and reaction (SILAR) technique [222]. A handfull of research has been devoted towards enhancing the performance of graphene to compete with platinum-based material and significant progress has been realized (Fig. 10). These studies have shown that TRGO formed at relatively higher temperatures are promising compared to CRGO or pristine graphene although very large

area networks of graphene material are needed when they are incorporated with the iodide/triiodide redox couple [223].

However, it is noteworthy to highlight that using thick layers of materials as electrodes could impose significant limitation to electron diffusion across the porous films network. Hence, with cobalt and sulfur-based mediators in graphene material, less quantity is used and lesser quantity is required for TRGO material [224]. In developing a low-cost material based on graphene, it is essential to dope the defect sites and edges in materials. However, graphene are can be used as hybrid material for solar cell incorporating iodide/triiodide redox couple. TRGO has shown to be a suitable option owing to its strong stabilization exhibited by nanoparticles at various defect sites [224].

7. Performance of graphene

The usefulness of graphene has been demonstrated in the extraction of photogenerated charge carriers from sensitizer such as quantum dots. The use of graphene practically fastens charge carrier generation, separation and transportation on absorption light energy in solar cell [225]. This has been found to support the extraction of photogenerated carriers in quantum dot sensitized solar cell [225]. A major issue con- fronting the use of carbon nanotubes in sensitized solar cells is their merging into bundles. Uniform distribution of QDs on graphene layer remedies this problem and thus, improves the perfor- mance of graphene-based solar cell [225].

As an optically transparent conducting materials (TCM), graphene allows the passage of light energy through the semiconduc- tor material and by this; serves as an ohmic contact for carrier transport in photovoltaic as well as transparent charge carrier [225, 226]. TCM comprises a layer of transparent conducting oxide (TCO) of indium tin oxide (ITO), fluorine doped tin oxide (FTO) or doped zinc oxide [227]. Carbon based films in the form of carbon nanotube and gra- phene has shown to be competitive low-cost TCM [228] with bandgap energies in the range 380–750 nm wavelengths. This implies that photon energy within the bandgap energy are absorbed with energies out the bandgap energy range are not collected rather visible light are allowed to pass through the scaffold to the absorber layer where they are absorbed to gen- erate chargers. Therefore, TCO materials with wider bandgap could eliminate the absorption of unwanted spectral wavelengths.

A single layer graphene (SLG) absorbs 2.3% fraction of light with a wide spectral bandwidth that allows for high velocities charge transfer [229-230]. The spectral absorption could also be modified by tuning the external electrical gating of a double-layer graphene to change the Fermi energy levels of graphene which also changes the absorption properties of the material [230,231]. The primary aim to alter the functionalization of a graphene stemmed from its short absorption wavelength depicting absence of photo- luminescence and can be resolved through enlarging the spectral bandgap energy by coupling graphene and a substrate. In addition, the presence of oxides alters the optoelectronic properties of graphene especially the adsorption to increase its catalytic properties [232,233]. Although the reactivity of graphene has not been fully outlined, however, pristine based graphene breaks sp2 bond to generate covalent bonds. In the adjacent regions to the break point,

reactivity is enhanced as well as in the geometrically strained regions [234]. However, it is remarkable that RGO and graphene oxide (GO) have oxygen groups that act as reactive regions. The performance of solar cell incorporated with graphene is as shown in Table 4. The incorporation of graphene based material has shown to transform dye and QDs solar cell performance upon optimization to absorb wider spectral wavelengths.

8. Graphene Applications in other types of solar cells

For many of the same reasons that they have been used in DSSCs, graphene materials have also been used in other types of solar cells. A brief overview is included here to provide context for the DSSC work. As mentioned in section 3.1, transparent conductors are a large potential market, and having cost-effective TCFs would allow improvements to conventional silicon solar cell technologies as well as to the thin film technologies (cadmium telluride, copper indium gallium selenide, organic, etc.), allowing for device structure modification, and a reduction in the number of silver contact lines on devices. Along these lines, a graphene material-based conductive ink could displace silver current collectors in the gamut of solar cell technologies. Currently, it is estimated that silver contact lines represent about $0.04/WP of devices and is highly dependent on the cost of silver [235]. Furthermore, most silver pastes currently marketed have to be sintered at elevated temperatures (>400 °C), increasing processing costs and limiting substrate selection. To be applicable, any replacement inks would have to achieve similar conductivity, both along the busbars and in contacting the device TCF without shading more of the device, a daunting task. In organic solar cells, graphene materials have been used as electron acceptors238 and hole conductors, which a few reviews summarize [236-238]. Additionally, graphene materials have been used to form Schottky junctions with $CdSe_2$, with the later device achieving $\eta > 8\%$. In line with this work, researchers have used graphene dispersions to facilitate stable growth of attached nanoparticles for quantum dot solar cells and for solar fuel applications [239-241]. Lastly, fundamental studies of graphene have shown hot carrier transport [242, 243]and multiple carrier generation from a single photon, [172] both effects which overcome the limits imposed on devices based on the band gap of semiconductors, and thus, a graphene photovoltaic device could obtain very high efficiencies in the future. Graphene materials have been used with a range of solar cell technologies, but what is distinguishing about DSSCs is that graphene materials, with their wide range of properties, have been used in almost all aspects of the device.

9. Conclusions and outlook

Although graphene materials can be used to improve DSSCs in a variety of roles, particular functions are best performed by specific graphene materials. Pristine graphene, followed by highly reduced graphene oxide, have the best prospects for transparent conductors, though by themselves the materials are not sufficient to meet application demands. These materials will have to either be electronically doped or exist as a part of a metal hybrid system. In the photoanode, graphene materials have resulted in improved photocurrent; however, it is unclear whether the advantages will apply to optimized devices. Whether graphene oxide, CRGO, or TRGO is processed with the TiO_2 is unlikely to mater

significantly, as heat treatment is generally required to sinter the TiO_2 layer, which will thermally reduce the graphene material. If there is a percolated graphene material network then sintering may not be necessary; however, each TiO_2 particle would have to be in contact with the graphene material network for best results. In this case, the sheets would have to be conducting and well dispersed through the TiO_2 matrix, so starting processing with graphene oxide and then reducing the material is a promising option. Pristine graphene could be advantageous in this application due to its high conductivity and relative inertness, but processing would be difficult, limiting application. Graphene materials can be used as a sensitizer in solar cells, and quantum effects, in particular, hot injection, could allow cells to exceed the Shockley"Queisser efficiency limit. Nevertheless, optimization processing of graphene quantum dots has brought the material closer to current organic dye structures. Graphene oxide could be a useful gelling agent in the electrolyte, whereas RGO in this role will likely catalyze recombination and reduce cell efficiency. At the cathode, two approaches have been shown that can equal or surpass the performance of platinum nanoparticles: (i) high surface area electrodes and (ii) high-activity materials. In both approaches RGO is advantageous as pristine graphene is relatively inert. In the first case, care must be taken to prevent restacking of sheets, while in the second, either a highly active nanoparticle composite can be formed or a redox mediator for which reduced graphene oxide is highly active (e.g., Co- (bpy)3(II/III)) can be used. Use of graphene materials in DSSCs has seen a rapid increase in research and fruitful results. Nevertheless, as research progresses, it is important to keep in mind that the various graphene materials have different properties integrally tied to their method of production¬[o] and each may be beneficial to different areas in a solar cell. A next stage of research, to bring graphene materials to higher relevance in the DSSC community, would be to study whether improvements discussed within this review can be carried over to the current best-in-class devices.

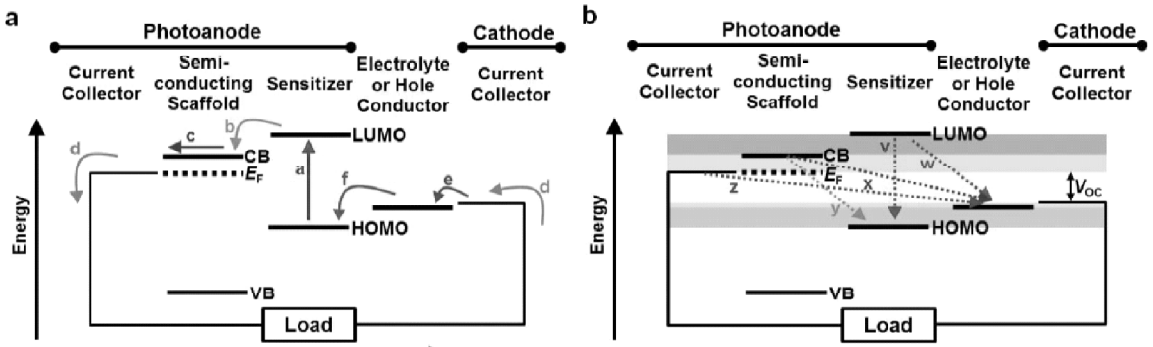

Figure 1: Energy diagram for a DSSC. CB and VB refer to the conduction band and valence band, respectively. EF represents the Fermi level of the semiconductor and is represented near CB due to a high level of electronic doping. LUMO and HOMO levels are the least unoccupied and highest unoccupied molecular orbitals of the sensitizer. For traditional DSSC architectures, at least one current collector must be a transparent electrode to allow light into the cell. (A) Desired electron pathway. Colored arrows a, b, c, d, e, and f represent some of the energy transfer steps as described in the main text. (B) Major recombination pathways. Colored arrows v, w, x, y, and z represent some parasitic recombination pathways. Voltage drops for different charge transfer steps are represented by the colored bands. Adapted with permission from ref 2. Copyright 2013 Joseph Roy-Mayhew.

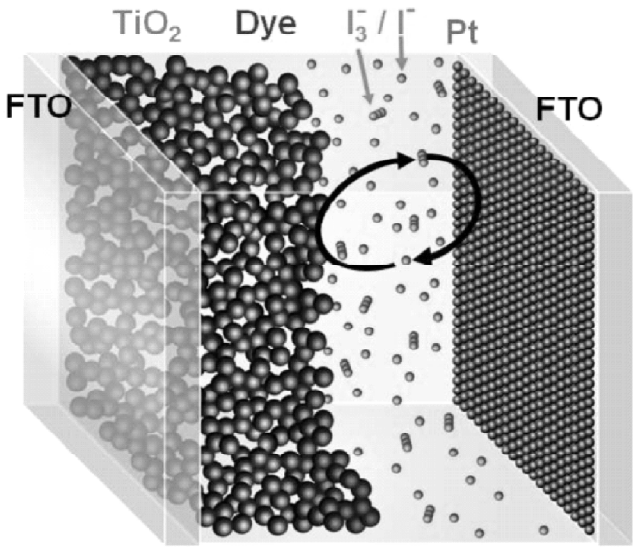

Figure 2: Schematic of a typical DSSC. The primary particle diameter of TiO_2 used is 10-20 nm, and the phase is anatase. Void space is about 50%. FTO generally has a sheet resistance of ~15 ©/sq and transmittance in the visible of ~ 85%. Platinum nanoparticles typically are created through thermolysis of chloroplatinic acid. Reprinted with permission from ref 2. Copyright 2013 Joseph Roy-Mayhew.

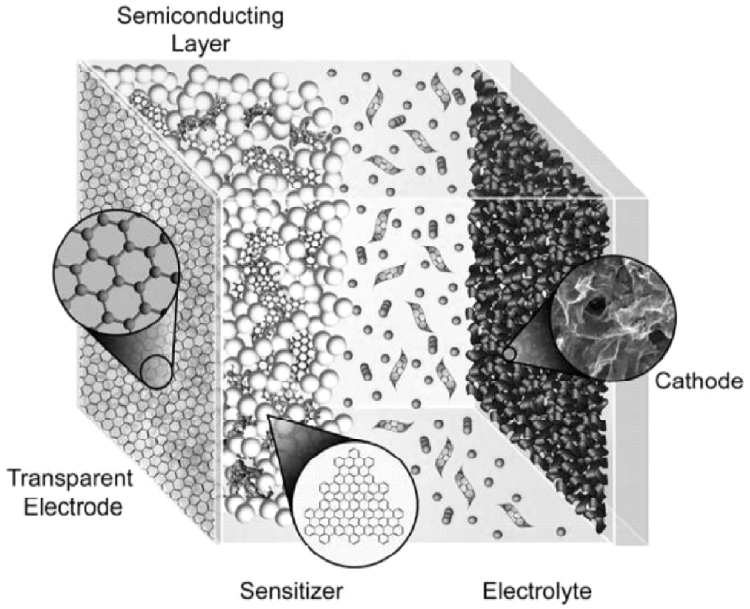

Figure 3: Schematic of a DSSC incorporating graphene materials in each part of the device. Numbers represent the section in which particular studies are discussed in this review. For instance, use of graphene materials as a transparent electrode for DSSCs is discussed in section 3.1. Adapted with permission from ref 2. Copyright 2013 Joseph Roy-Mayhew.

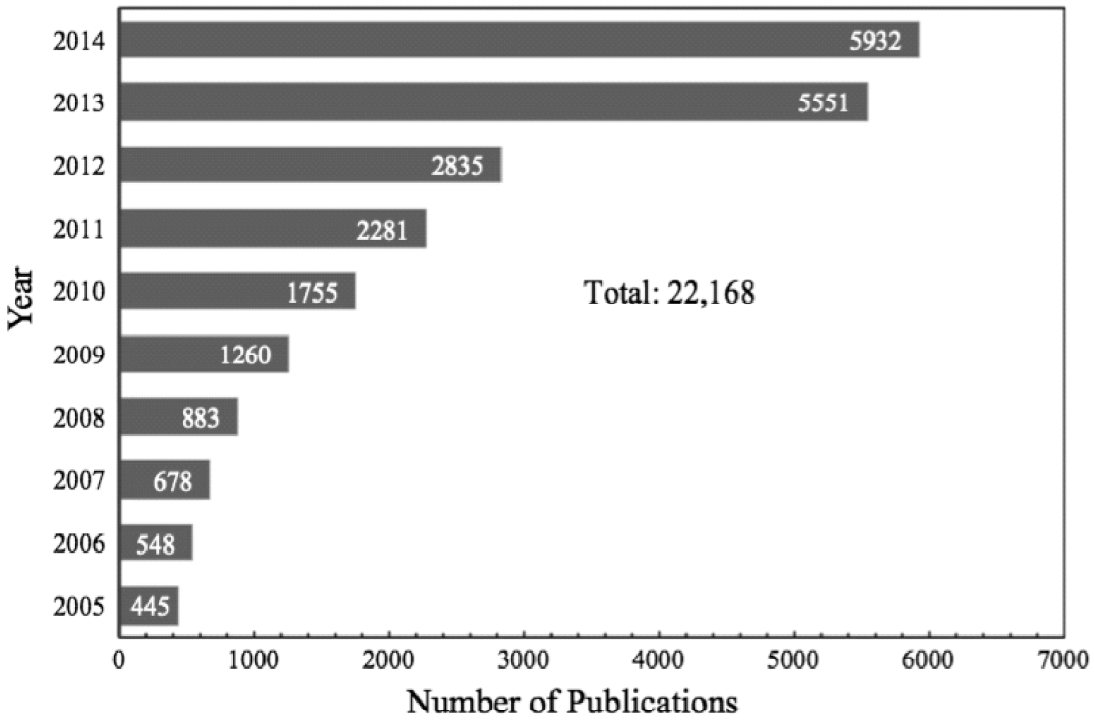

Figure 4: Number of publications published per year from literature search using the keywords "dye sensitized" and "solar" (data source ISI Web of Knowledge).

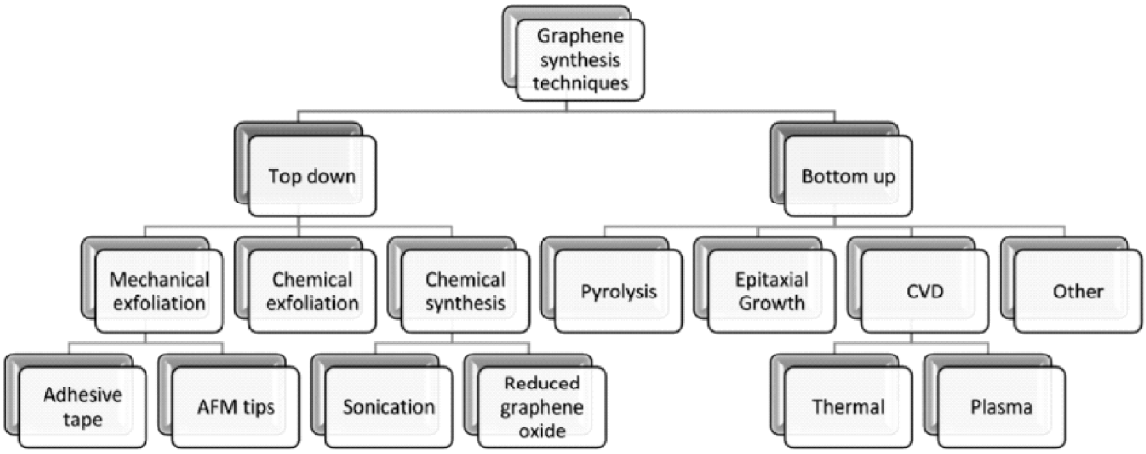

Figure 5: A process flow chart of Graphene synthesis

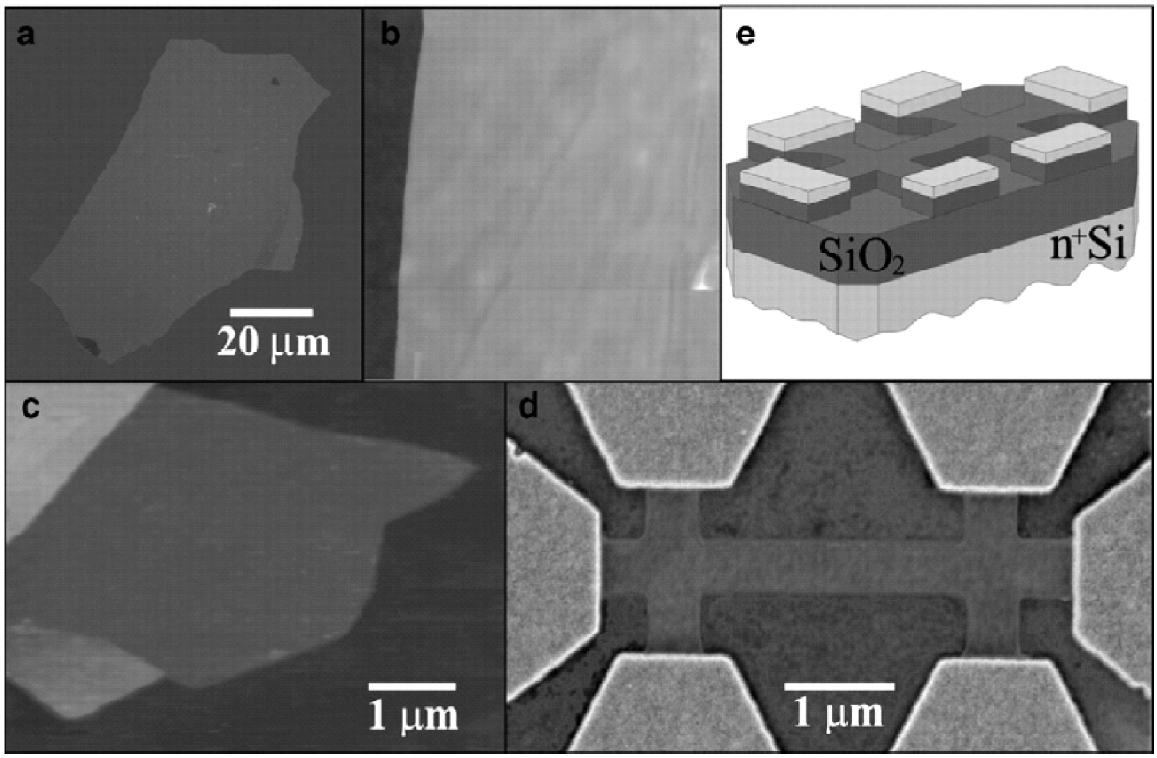

Figure 6: Graphene films. a Photograph (in normal white light) of a relatively large multilayer graphene flake with thickness *3 nm on top of an oxidized Si wafer. b Atomic force microscope (AFM) image of 2 lm by 2 μm area of this flake near its edge. Colors: dark brown, SiO2 surface; orange, 3 nm height above the SiO_2 surface. c AFM image of single-layer graphene. Colors: dark brown, SiO2 surface; brown–red (central area), 0.8 nm height; yellow–brown (bottom left), 1.2 nm; orange (top left), 2.5 nm. d Scanning electron microscope image of FLG (Few layer graphene). e Schematic view of the device in (D)

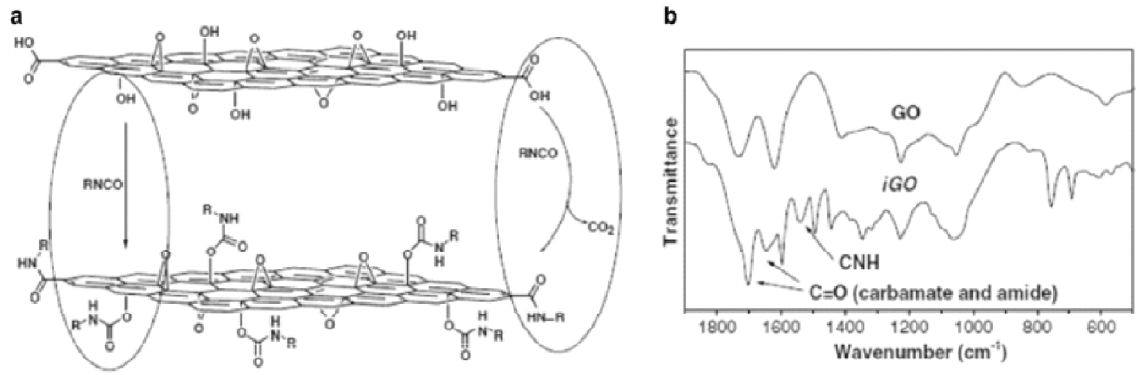

Figure 7: Proposed reactions during the isocyanate treatment of GO where organic isocyanates react with the hydroxyl (left oval) of graphene oxide sheets to form carbamate and amide functionalities, respectively. b FT-IR spectra of GO and isocyanate-treated GO.

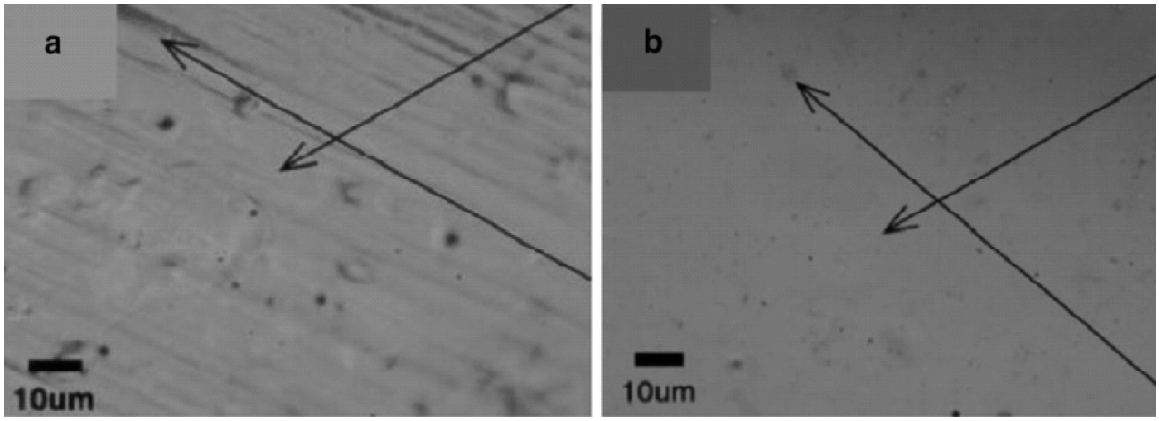

Figure 8: a Optical image of as grown graphene on copper, the corrugations on metal foil are indicated by black arrows. b Same graphene when shifted to 300 nm SiO2. Here dark purple areas highlighted by black arrows displays that even on low carbon solubility metal like copper, corrugations on starting substrate can result in formation of significant multilayer regions along with monolayer graphene [45]. Li *et al.* used CVD process to produce large-scale monolayer graphene on copper foils. 25 lm thick copper foils were first heated to 1000 ° C in a flow of 2 sccm (standard cubic centimeters per minute) hydrogen at low pressure and then exposed to methane flow of 35 sccm and pressure of 500mTorr and acquired sheet resistances of 125X/W for a single layer. Using a repeated transfer method, doped 4-layer graphene sheets were formed with sheet resistances as low as 30X/W and optical transmittance greater than 90%. These 4-layer graphene sheets are better to commercially accessible indium tin oxide (ITO). Permission from [146]

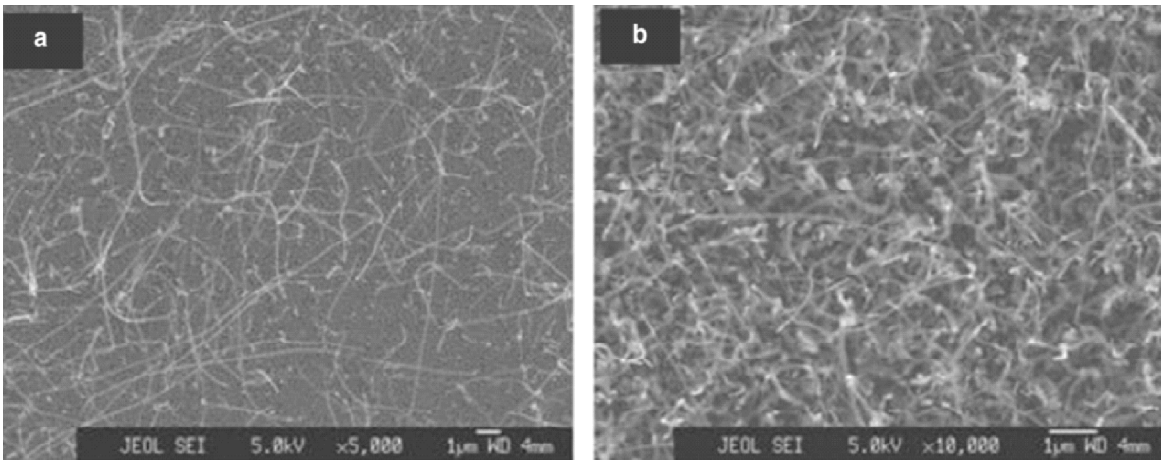

Figure 9: SEM images of sample by CVD growth method on Ni film at 900–1000 °C at various H : CH ratios with permission of [154]

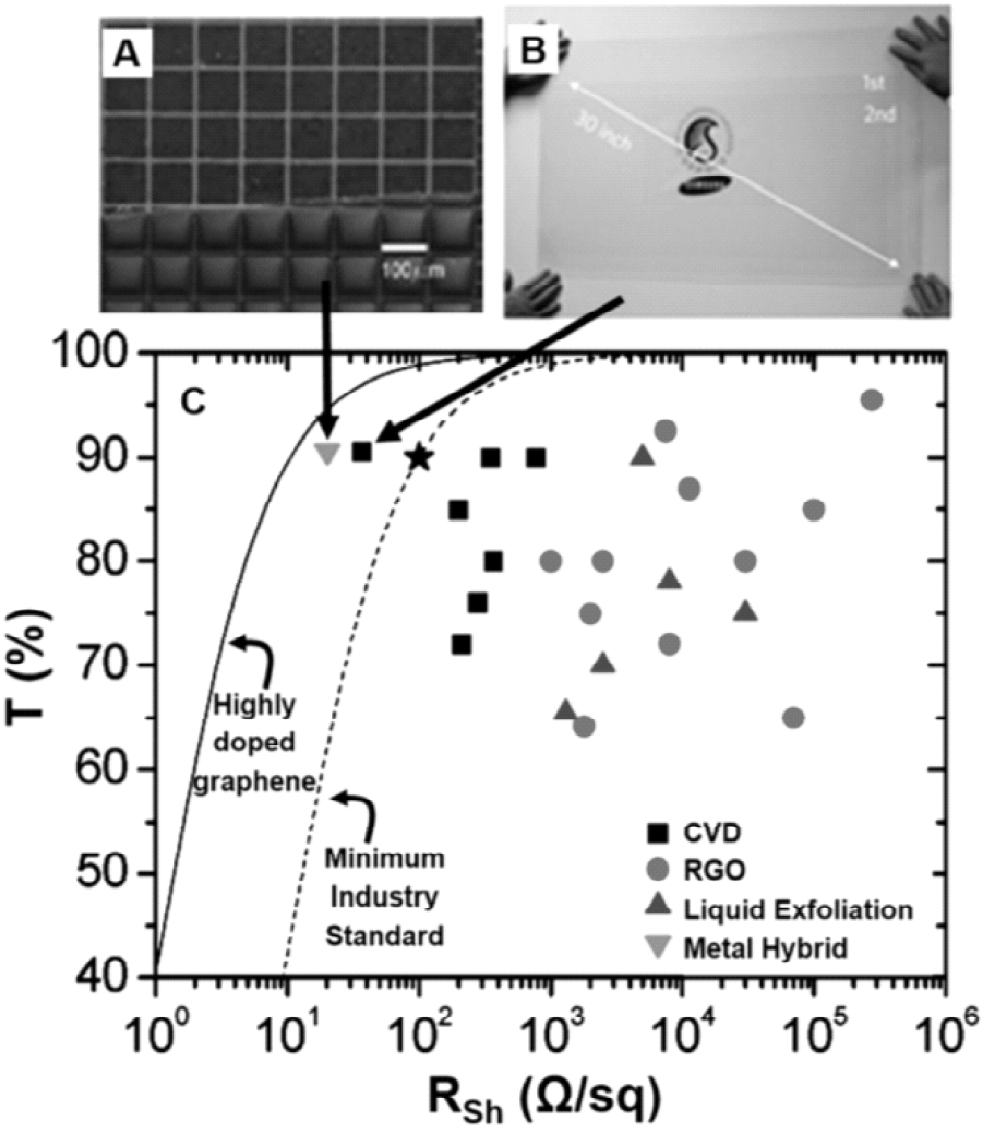

Figure 10: Overview of graphene materials in transparent electrodes. (A) Metal grid coated with CVD-derived graphene film. Adapted with permission from ref 124. Copyright 2011 American Chemical Society. (B) Large area HNO3 electronically doped CVD-derived graphene film. Adapted by permission from Macmillan Publishers Ltd. Nature Nanotechnology from ref 120, copyright 2010. (C) Compilation of transparent films. Adapted with permission from ref 115. Copyright 2010 American Chemical Society. Dotted line represents σDC/σOp = 35, with the star representing RSh = 100 Ω/sq at T = 90%. The solid line represents σDC/σOp = 330, a value calculated for highly electronically doped pristine graphene.

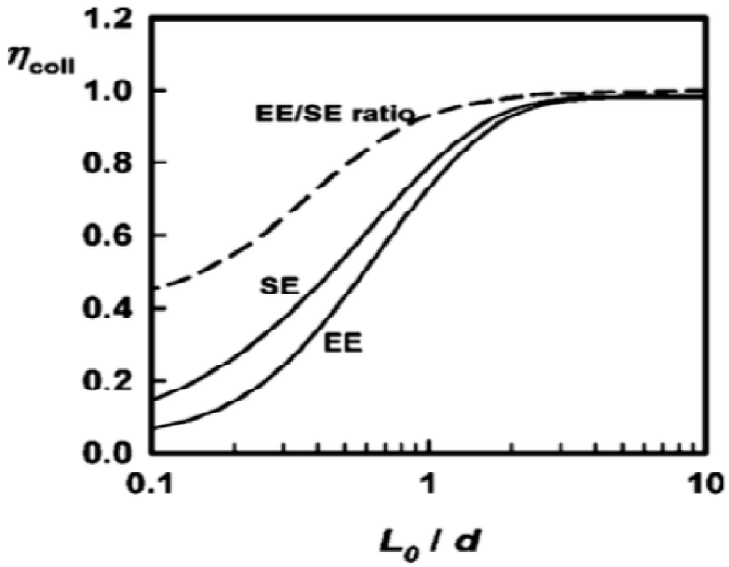

Figure 11: Charge collection in the photoanode. ·coll is the charge collection efficiency, the SE curve represents collection when the device is illuminated from the front (through transparent conductor), while EE represents illumination from the rear (though counter electrode and electrolyte). L0 is the path length to the current collector, and d is the electron diffusion length in the material. Thus, using this model, an electron generated 10 μm from the current collector in a TiO2 film which had a 20 ¼m diffusion length would reach the current collector about 90% of the time (~ 10% of the electrons would recombine). Reproduced with permission from ref 148. Copyright 2009 American Chemical Society.

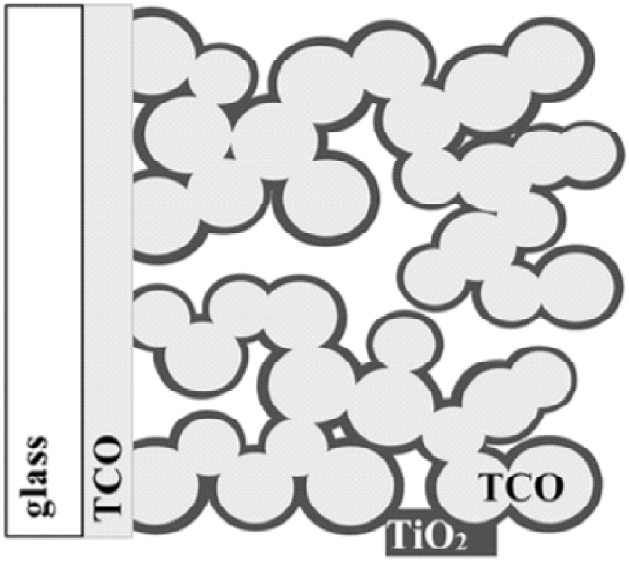

Figure 12: Schematic of a nanoporous transparent conducting oxide (TCO) acting as the electrode to reduce the collection length. Most of the volume is taken up by the TCO, limiting the amount of TiO2 and surface area available for dye adsorption. Reproduced with permission from ref 150. Copyright 2005 American Chemical Society.

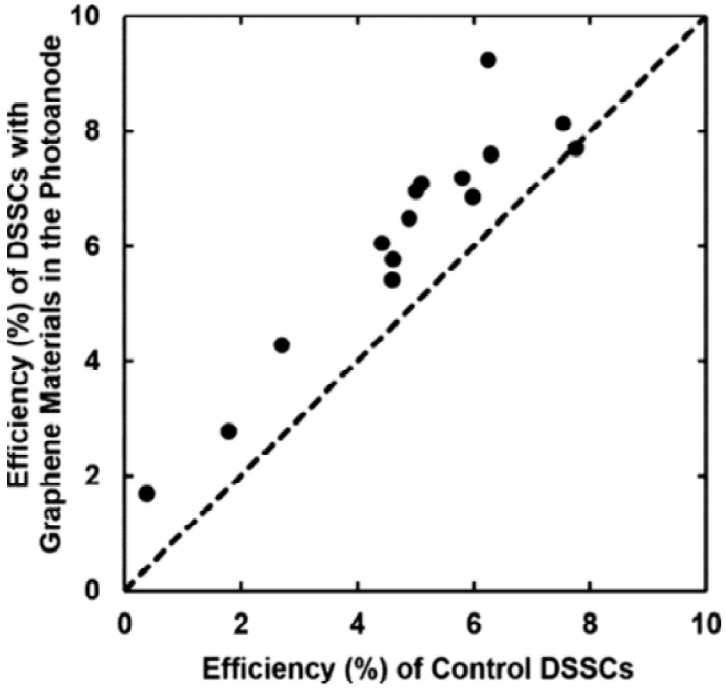

Figure 13: Comparison of reported efficiencies for DSSCs with and without graphene materials in the TiO2 scaffold layer.

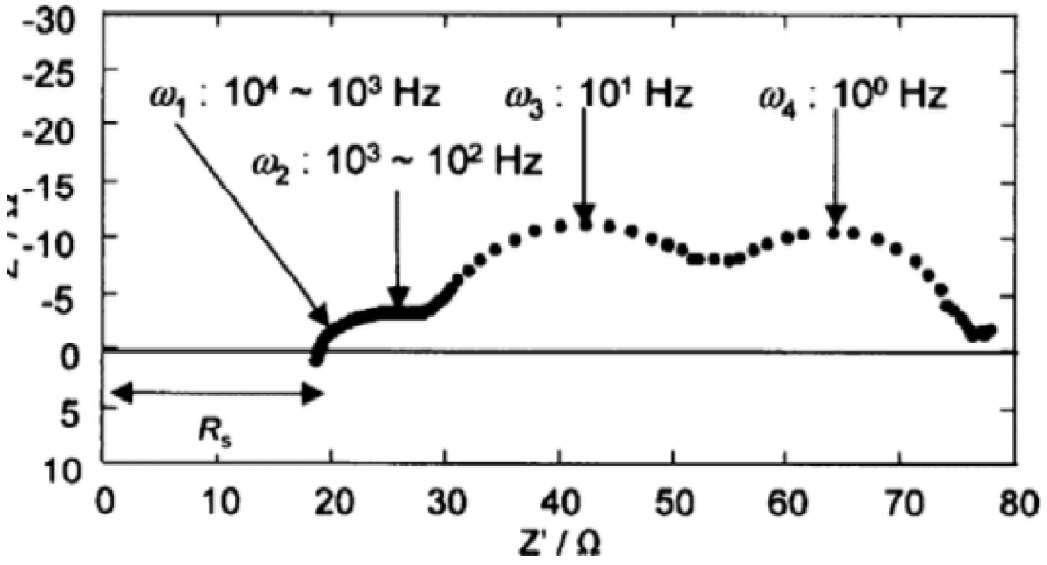

Figure 14: Sample EIS spectra of full DSSC under light. Often, as a result of DSSC fabrication techniques, only two of these features can be discerned during testing. Adapted from J. Electrochem. Soc. 2005, 152, E69. Copyright 2005 ECS-The Electrochemical Society (ref 157).

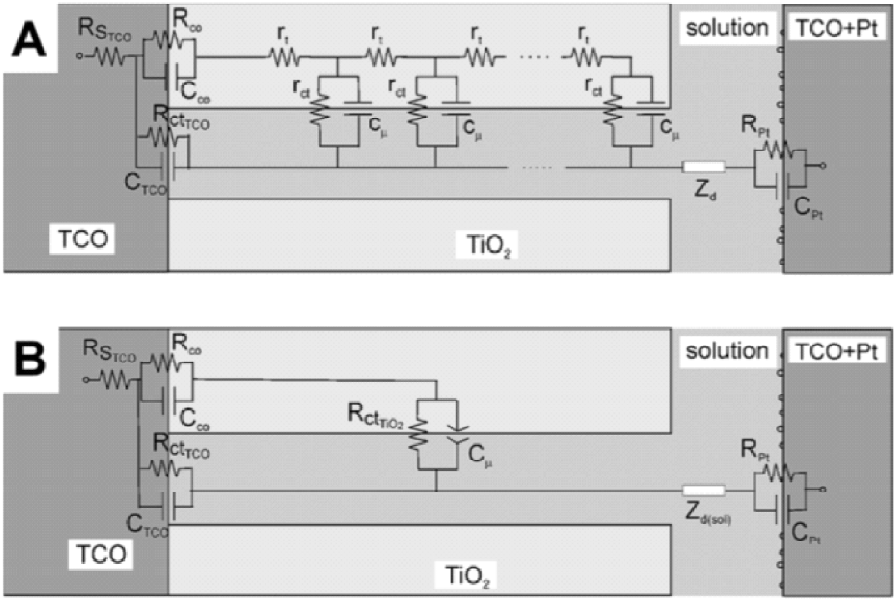

Figure 15: EIS equivalent circuits for DSSCs (A) in the dark and (B) under illumination. Reproduced with permission from ref 162. Copyright 2007 American Chemical Society.

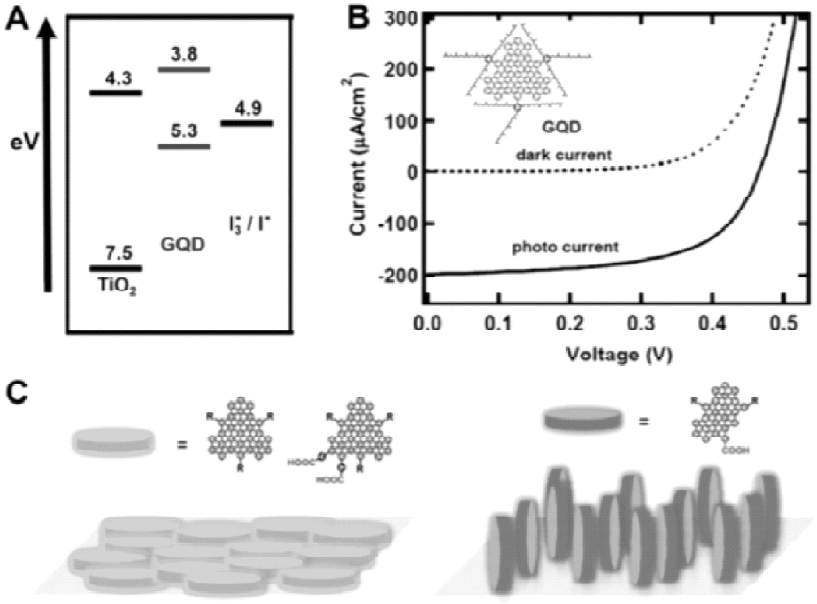

Figure 16: GO photovoltaic performance. (A) Energy level diagram versus the iodide/triiodide redox couple and anatase phase TiO_2. (B) Photovoltaic performance of a GO-sensitized DSSC. (Inset) Structure of the GO used for sensitization. (A and B) Adapted with permission from ref 27. Copyright 2010 American Chemical Society. (C) Schematic of vertical and horizontal orientation of GO. Reproduced with permission from ref 176. Copyright 2011 American Chemical Society.

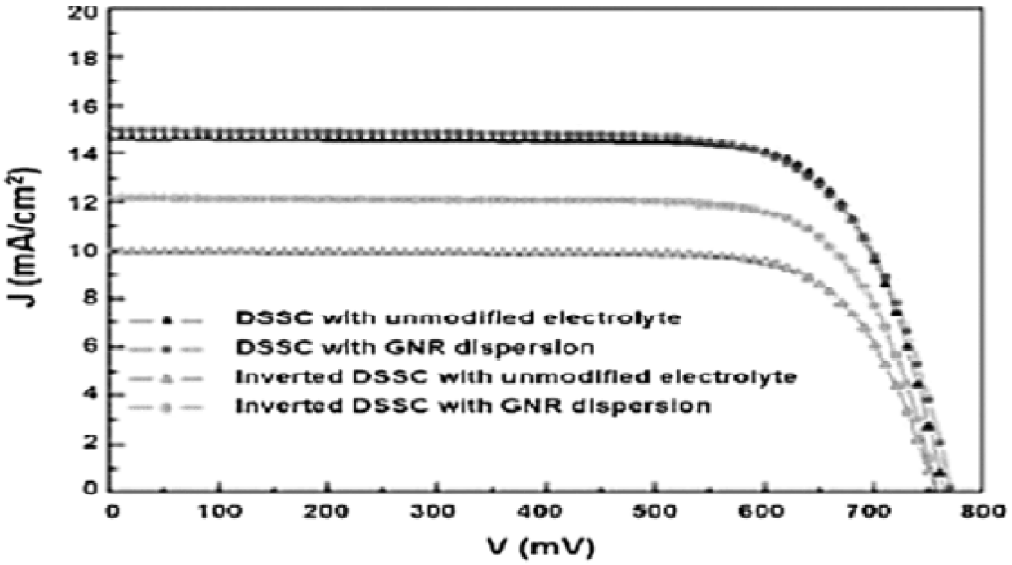

Figure 17: Photo-induced transparency of iodide/triiodide electrolyte using graphene nano-ribbons depicting J–V curves of the inverted architect of illuminated DSSCs with and without graphene nano-ribbons.

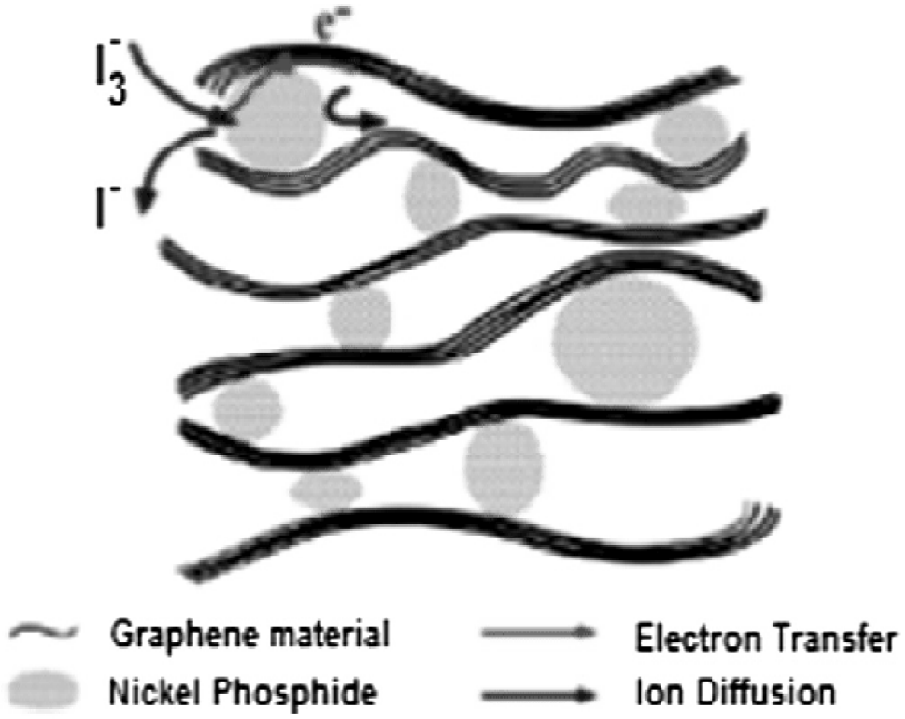

Figure 18: 3 μm thick graphene material) Schematic graphene materials used as conductive scaffolds for high-activity materials. Adapted from Wan *et al.* (2011), Dou *et al.* (2012).

Table 1
Concise history of Bottom up graphene

Method	*Typical dimension*		*Advantage*	*Disadvantage*	*Ref.*
Thickness		*Lateral*			
Confined self-assembly	Single layer	100's nm	Thickness control	Existence of defects	[37]
CVD	Few layer	Very large (cm)	Large size; high quality	Small production scale	[17, 38–42]
Arc discharge	Single, bi and few layers	Few 100 nm to a few μm	Can produce ≈10 g/h of graphene	Low yield of graphene; carbonaceous impurities	[43, 44]
Epitaxial growth on SiC	Few layers	Up to cm size	Very large area of pure graphene	Very small scale	[45–51]
Unzipping of carbon nanotubes	Multiple layers	few μm long nano ribbons	Size controlled by selection of the starting nanotubes	Expensive starting material; oxidized graphene	[33, 34, 52]
Reduction of CO	Multiple layers	Sub-μm	Un-oxidized sheets	Contamination with a-Al2O3 and a-Al2S	[53]

Table 2
Concise history of Top-down graphene

Method	*Typical dimension*		*Advantage*	*Disadvantage*	*Ref.*
	Thickness	*Lateral*			
Micromechanical exfoliation	Few layers	lm to cm	Large size and unmodified graphene sheets	Very small scale production	[15]
Direct sonication of graphite	Single and multiple layers	lm or sub-lm	Unmodified graphene, inexpensive	Low yield; separation	[54,55]
Electrochemical exfoliation/functionalization of graphene	Single and few layers	500–700 nm	Single step functionalization and exfoliation; high electrical conductivity of the functionalized graphene	Cost of ionic liquids	[56]
Super acid dissolution of graphite	Mostly single layer	300–900 nm	Unmodified graphene; scalable	Use of hazardous chlorosulfonic acid; cost of acid removal	[57]

Table 3
Minimum concentration of graphene oxide for gelation at 23 °C for solvents containing 4 Mm tetramethylammonium tetrafluoroboratea

Solvent	*Graphene concentration (wt.%)*
1-Butanol	0.35
Tetrahydrofuran	0.37
1-Pentanol	0.4
Acetonitrile	0.4
Ethanol	0.57
Water	0.8
Diethylene glycol	1.4

Table 4
Performance of sensitized solar cell incorporated with graphene

Sample	*Content of graphene (wt.%)*	*JSC (mA/cm2)*	*Voc (V)*	*FF*	*η(%)*	*Ref*
Scaffold layer with T-CRGO	0.6	16.30	0.69	0.62	7.0	[234]
Scaffold layer with TRGO (solvothermal)	0.8	13.20	0.72	0.73	7.1	[235]
$TiCl_4$-derived undercoat, scaffold layer with CRGO	0.02	19.30	0.74	0.53	7.5	[236]
Scaffold layer with graphene oxide	0.8	13.60	0.76	0.75	7.7	[237]
Control (including $TiCI_4$-derived underlayer, TiCl4-derivedovercoat, and scattering layer)	0	13.30	0.77	0.76	7.8	[238]
Underlayer with TRGO, scaffold layer with CRGO	0.02	19.50	0.75	0.56	8.1	[240]
Cu_2S-rGO-PVAbinder/FTO	-	18.40	0.52	46	4.40	[241]

Reference

[1] Smalley RE. Future global energy prosperity: the terawatt challenge. MRS Bull 2005; 30: 412–7.

[2] Bahnemann D. Photocatalytic water treatment: solar energy applications. Sol Energy 2004; 77: 445–59.

[3] Grossman GM, Krueger AB. Economic growth and the environment. USA: National Bureau of Economic Research, MIT press; 1994.

[4] Faninger G. The potential of solar heat in the future energy system. Austria: IFF- University of Klagenfurt; 2010.

[5] Aleklett K, Campbell CJ. The peak and decline of world oil and gas production. Miner Energy-Raw Mater Rep 2003; 18: 5–20.

[6] Pandey A, Tyagi V, Jeyraj A, Selvaraj L, Rahim N, Tyagi S. Recent advances in solar photovoltaic systems for emerging trends and advanced applications. Renew Sustain Energy Rev 2016; 53: 859–84.

[7] Green MA, Emery K, Hishikawa Y, Warta W, Dunlop ED. Solar cell efficiency tables (version 47). Prog Photovolt: Res Appl 2016: 24.

[8] O'regan B, Grfitzeli M. A low-cost, high-efficiency solar cell based on dye- sensitized. Nature 1991; 353: 737–40.

[9] Green MA. Thin-film solar cells: review of materials, technologies and commercial status. J Mater Sci: Mater Electron 2007; 18: 15–9.

[10] Halme J. Dye-sensitized nanostructured and organic photovoltaic cells: technical review and preliminary tests. Department of Engineering Physics and Mathematics; 2002. p. 115.

[11] Kakiage K, Aoyama Y, Yano T, Otsuka T, Kyomen T, Unno M, et al. An achievement of over 12% efficiency in an organic dye-sensitized solar cell. Chem Commun 2014; 50: 6379–81.

[12] GraetzelM,JanssenRA,MitziDB,SargentEH.Materialsinterfaceengineeringfor solution-processed photovoltaics. Nature 2012; 488: 304–12.

[13] Rani S, Suri P, Shishodia P, Mehra R. SynthesisofnanocrystallineZnOpowdervia sol–gel route for dye-sensitized solar cells. Sol Energy Mater Sol Cells 2008; 92: 1639–45.

[14] Byranvand MM, Kharat AN, Badiei A, Bazargana M. Electron transfer in dye- sensitized solar cells. J Optoelectron Biomed Mater 2012; 4: 49–57.

[15] Koyama Y, Miki T, Wang X-F, Nagae H. Dye-sensitized solar cells based on the principles and materials of photosynthesis: mechanisms of suppression and enhancement of photocurrent and conversion efficiency. Int J Mol Sci 2009; 10: 4575–622.

[16] Zhu K, Neale NR, Miedaner A, Frank AJ. Enhanced charge-collection efficiencies and light scattering in dye-sensitized solar cells using oriented TiO2 nanotubes arrays. Nano Lett 2007; 7: 69–74.

[17] Koo HJ, Kim YJ, Lee YH, Lee WI, Kim K, Park NG. Nano embossed hollow spherical TiO2 as bifunctional material for high efficiency dye sensitized solar cells. Adv Mater 2008; 20: 195–9.

[18] Park JH, Jung SY, Kim R, Park N-G, Kim J, Lee S-S. Nanostructured photoelec- trode consisting of TiO2 hollow spheres for non-volatile electrolyte-based dye-sensitized solar cells. J Power Sources 2009; 194: 574–9.

[19] Bakhshayesh A, Mohammadi M, Fray D. Controlling electron transport rate and recombination process of TiO2 dye-sensitized solar cells by design of double-layer films with different arrangement modes. Electrochim Acta 2012; 78: 384–91.

[20] Qiu Y, Chen W, Yang S. Double layered photoanodes from variable size anatase TiO2 nanospindles: a candidate for high efficiency dye sensitized solar cells. Angew Chem 2010; 122: 3757–61.

[21] FuQ, SunW. Mietheory for light scatteringb a spherical particle in an absorbing medium. Appl Opt 2001; 40: 1354–61.

[22] Wang L, Jacques SL, Zheng L.MCML— of light transport in multi-layered tissues. Comput Methods Prog Biomed 1995; 47: 131–46.

[23] Billmeyer FW, Chassaigne PG, Dubois JF. Determining pigment optical properties for use in the Mie and many flux theories. Color Res Appl 1980; 5: 108–12.

[24] Anderson NA, Lian T. Ultrafast electron injection from metal polypyridyl com- plexes to metal-oxide nanocrystalline thin films. Coord Chem Rev 2004; 248: 1231–46.

[25] Zhang S, Yang X, Qin C, Numata Y, Han L. Interfacial engineering for dye-sensitized solar cells. J Mater Chem A 2014; 2: 5167–77.

[26] Cameron PJ, Peter LM. Characterization of titanium dioxide blocking layers in dye-sensitized nanocrystalline solar cells. J Phys Chem B 2003; 107: 14394–400.

[27] Lee S-W, Ahn K-S, Zhu K, Neale NR, Frank AJ. Effects of TiCl4 treatment of nanoporous TiO2 films on morphology, light harvesting, and charge-carrier dynamics in dye-sensitized solar cells. J Phys Chem C 2012; 116: 21285–90.

[28] Sedghi A, Miankushki HN. Influence of TiCl4 treatment on structure and performance of dye-sensitized solar cells. Jpn J Appl Phys 2013; 52: 075002.

[29] Xia J, Masaki N, Jiang K, Wada Y, Yanagida S. Importance of blocking layers at conducting glass/TiO2 interfaces in dye-sensitized ionic-liquid solar cells. Chem Lett 2006; 35: 252–3.

[30] Kim YJ, Kim KH, Kang P, Kim HJ, Choi YS, Lee WI. Effect of layer-by-layer assembled SnO2 interfacial layers in photovoltaic properties of dye-sensitized solar cells. Langmuir 2012; 28: 10620–6.

[31] Roy-Mayhew JD, Aksay IA. Graphene materials and their use in dye-sensitized solar cells. Chem Rev 2014; 114: 6323–48.

[32] Sommeling P,O'regan B,HaswellR, SmitH, BakkerN, Smits J,etal.Influenceof a TiCl4 post-treatment on nanocrystalline TiO2 films in dye-sensitized solar cells. J Phys Chem B 2006; 110: 19191–7.

[33] Jung HS, Lee J-K, Nastasi M, Lee S-W, Kim J-Y, Park J-S, et al. Preparation of nanoporous MgO-coated TiO2 nanoparticles and their application to the electrode of dye-sensitized solar cells. Langmuir 2005; 21: 10332–5.

[34] Palomares E, Clifford JN, Haque SA, Lutz T, Durrant JR. Control of charge recombination dynamics in dye sensitized solar cells by the use of conformally deposited metal oxide blocking layers. J Am Chem Soc 2003; 125: 475–82.

[35] Bandara J, Pradeep U. Tuning of the flat-band potentials of nanocrystalline TiO2 and SnO2 particles with an outer-shell MgO layer. Thin Solid Films 2008; 517: 952–6.

[36] Prasittichai C, Hupp JT. Surface modification of SnO2 photoelectrodes in dye- sensitized solarcells: significant improvements in photovoltage via Al2O3 atomic layer deposition. J Phys Chem Lett 2010; 1: 1611–5.

[37] Wang Z-S, Yanagida M, Sayama K, Sugihara H. Electronic-insulating coating of CaCO3 on TiO2 electrode in dye-sensitized solar cells: improvement of electron lifetime and efficiency. Chem Mater 2006; 18: 2912–6.

[38] Okada N, Karuppuchamy S, Kurihara M. An efficient dye-sensitized photoelec-trochemical solar cell made from CaCO3-coated TiO2 nanoporous film. Chem Lett 2005; 34: 16–7.

[39] Chen S-G, Chappel S, Diamant Y, Zaban A. Preparation of Nb2O5 coated TiO2nanoporous electrodes and their application in dye-sensitized solar cells. Chem Mater 2001; 13: 4629–34.

[40] Menzies DB, Cervini R, Cheng Y-B, Simon GP, Spiccia L. Nanostructured ZrO2-coated TiO2 electrodes for dye-sensitised solar cells. J Sol-Gel Sci Technol 2004; 32: 363–6.

[41] Zhang J, Zaban A. Efficiency enhancement in dye-sensitized solar cells by in situ passivation of the sensitized nanoporous electrode with Li2CO3. Electrochim Acta 2008; 53: 5670–4.

[42] Motahari S. Surface passivation of CIGS solar cells by atomic layer deposition; 2013.

[43] Babu DD, Cheema H, Elsherbiny D, El-Shafei A, Adhikari AV. Molecular engineering and theoretical investigation of novel metal-free organic chromo-phores for dye-sensitized solar cells. Electrochim Acta 2015; 176: 868–79.

[44] Tien T-C, Pan F-M, Wang L-P, Lee C-H, Tung Y-L, Tsai S-Y, et al. Interfacial energy levels and related properties of atomic-layer-deposited Al2O3 films on nanoporous TiO2 electrodes of dye-sensitized solar cells. Nanotechnology 2009; 20: 305201.

[45] Shanmugam M, Baroughi MF, Galipeau D. Effect of atomic layer deposited ultra thin HfO2 and Al2O3 interfacial layers on the performance of dye sensitized solar cells. Thin Solid Films 2010; 518: 2678–82.

[46] SonS, HwangSH, KimC, YunJY, JangJ. Designedsynthesis of SiO2/TiO2core/shell structure as light scattering material for highly efficient dye-sensitized solar cells. ACS Appl Mater Interfaces 2013; 5: 4815–20.

[47] Hara K, Dan-oh Y, Kasada C, Ohga Y, Shinpo A, Suga S, et al. Effect of additives on the photovoltaic performance of coumarin-dye-sensitized nanocrystalline TiO2 solar cells. Langmuir 2004; 20: 4205–10.

[48] Xia J, Li F, Huang C, Zhai J, Jiang L. Improved stability quasi-solid-state dye-sensitized solar cell based on polyether framework gel electrolytes. Sol Energy Mater Sol Cells 2006; 90: 944–52.

[49] Biancardo M, West K, Krebs FC. Quasi-solid-state dye-sensitized solar cells: Pt and PEDOT: PSS counter electrodes applied to gel electrolyte assemblies. J Photochem Photobiol A: Chem 2007; 187: 395–401.

[50] Li B, Wang L, Kang B, Wang P, Qiu Y. Review of recent progress in solid-state dye-sensitized solar cells. Sol Energy Mater Sol Cells 2006; 90: 549–73.

[51] Wang P, Zakeeruddin SM, Exnar I, Gratzel M. High efficiency dye-sensitized nanocrystalline solar cells based on ionic liquid polymer gel electrolyte. Chem Commun 2002: 2972–3.

[52] Wang P, Zakeeruddin SM, Moser J-E, Gratzel M. A new ionic liquid electrolyte enhances the conversion efficiency of dye-sensitized solar cells. J Phys Chem B 2003; 107: 13280–5.

[53] Mathew S, Yella A, Gao P, Humphry-Baker R, Curchod BF, Ashari-Astani N, et al. Dye-sensitized solar cells with 13% efficiency achieved through the molecular engineering of porphyrin sensitizers. Nat Chem 2014; 6: 242–7.

[54] Kakiage K, Aoyama Y, Yano T, Oya K, Fujisawa J-I, Hanaya M. Highly-efficient dye-sensitized solar cells with collaborative sensitization by silyl-anchor and carboxy-anchor dyes. Chem Commun 2015; 51: 15894–7.

[55] Redmond G, Fitzmaurice D, Graetzel M. Visible light sensitization by cis-bis (thiocyanato) bis (2, 22 -bipyridyl-4, 42 -dicarboxylato) ruthenium(II) of a trans- parent nanocrystalline ZnO film prepared by sol-gel techniques. Chem Mater 1994; 6: 686–91.

[56] Dinh NN, Bernard M-C, Hugot-Le Goff A, Stergiopoulos T, Falaras P. Photoelectrochemical solar cells based on SnO2 nanocrystalline films. Comptes Rendus Chim 2006; 9: 676–83.

[57] Ou JZ, Rani RA, Ham M-H, Field MR, Zhang Y, Zheng H, et al. Elevated temperature anodized Nb2O5: a photoanode material with exceptionally large photoconversion efficiencies. ACS Nano 2012; 6: 4045–53.

[58] Gholamrezaei S, Niasari MS, Dadkhah M, Sarkhosh B. New modified sol–gel method for preparation SrTiO3 nanostructures and their application in dye- sensitized solar cells. J Mater Sci: Mater Electron 2016; 27: 118–25.

[59] Tan B, Toman E, Li Y, Wu Y. Zinc stannate (Zn2SnO4) dye-sensitized solar cells. J Am Chem Soc 2007; 129: 4162–3.

[60] Hara K, Zhao Z-G, Cui Y, Miyauchi M, Miyashita M, Mori S. Nanocrystalline electrodes based on nanoporous-walled WO3 nanotubes for organic-dye-sensi- tized solar cells. Langmuir 2011; 27: 12730–6.

[61] Serpone N, Lawless D, Khairutdinov R. Size effects on the photophysical proper- ties of colloidal anatase TiO2 particles: size quantization versus direct transitions in this indirect semiconductor?. J Phys Chem 1995; 99: 16646–54.

[62] Wang Y, Hao Y, Cheng H, Ma J, Xu B, Li W, et al. The photoelectrochemistry of transition metal-ion-doped TiO2 nanocrystalline electrodes and higher solar cell conversion efficiency based on Zn2+-doped TiO2 electrode. J Mater Sci 1999; 34: 2773–9.

[63] Zhang X, Liu F, Huang Q-L, Zhou G, Wang Z-S. Dye-sensitized W-doped TiO2 solar cells with a tunable conduction band and suppressed charge recombination. J Phys Chem C 2011; 115: 12665–71.

[64] Ko KH, Lee YC, Jung YJ. Enhanced efficiency of dye-sensitized TiO 2 solar cells (DSSC) by doping of metal ions. J Colloid Interface Sci 2005; 283: 482–7.

[65] Zhang J, Zhao Z, Wang X, Yu T, Guan J, Yu Z, et al. Increasing the oxygen vacancy density on the TiO2 surface by La-doping for dye-sensitized solar cells. J Phys Chem C 2010; 114: 18396–400.

[66] Lu X, Mou X, Wu J, Zhang D, Zhang L, Huang F, et al. Improved performance dye sensitized solar cells using Nb doped TiO2 electrodes: efficient electron injection and transfer. Adv Funct Mater 2010; 20: 509–15.

[67] Ma T, Akiyama M, Abe E, Imai I. High-efficiency dye-sensitized solar cell based on a nitrogen-doped nanostructured titania electrode. Nano Lett 2005; 5: 2543–7.

[68] Kang SH, Kim HS, Kim J-Y, Sung Y-E. Enhanced photocurrent of nitrogen-doped TiO2 film for dye-sensitized solar cells. Mater Chem Phys 2010; 124: 422–6.

[69] Chu D, Yuan X, Qin G, Xu M, Zheng P, Lu J, et al. Efficient carbon-doped nanostructured TiO2 (anatase) film for photoelectrochemical solar cells. J Nanopart Res 2008; 10: 357–63.

[70] Song J, Yang HB, Wang X, Khoo SY, Wong C, Liu X-W, et al. Improved utilization of photogenerated charge using fluorine-doped TiO2 hollow spheres scattering layer in dye-sensitized solar cells. ACS Appl Mater Interfaces 2012; 4: 3712–7.

[71] Sun Q, Zhang J, Wang P, Zheng J, Zhang X, Cui Y, et al. Sulfur-doped TiO2 nanocrystalline photoanodes for dye-sensitized solar cells. J Renew Sustain Energy 2012; 4: 023104.

[72] Wang W, Liu Y, Sun J, Gao L. Nitrogen and yttrium co-doped mesoporous titania photoanodes applied in DSSCs. J Alloy Compd 2016; 659: 15–22.

[73] Zhang J, Peng W, Chen Z, Chen H, Han L. Effect of cerium doping in the TiO2 photoanode on the electron transport of dye-sensitized solar cells. J Phys Chem C 2012; 116: 19182–90.

[74] Xie Y, Huang N, You S, Liu Y, Sebo B, Liang L, et al. Improved performance of dye- sensitized solar cells by trace amount Cr-doped TiO2 photoelectrodes. J Power Sources 2013; 224: 168–73.

[75] Shogh S, Mohammadpour R, Taghavinia N. Improved photovoltaic performance of nanostructured solar cells by neodymium-doped TiO2 photoelectrode. Mater Lett 2015; 159: 273–5.

[76] Mehmood U, Hussein IA, Harrabi K, Mekki M, Ahmed S, Tabet N. Hybrid TiO2– multiwall carbon nanotube (MWCNTs) photoanodes for efficient dye sensitized solar cells (DSSCs). Sol Energy Mater Sol Cells 2015; 140: 174–9.

[77] Ako RT, Ekanayake P, Tan AL, Young DJ. La modified TiO2 photoanode and its effect on DSSC performance: a comparative study of doping and surface treatment on deep and surface charge trapping. Mater Chem Phys 2016; 172: 105–12.

[78] Tanyi AR, Rafieh AI, Ekaneyaka P, Tan AL, Young DJ, Zheng Z, et al. Enhanced efficiency of dye-sensitized solar cells based on Mg and La co-doped TiO2 photoanodes. Electrochim Acta 2015; 178: 240–8.

[79] Wang Z-S, Kawauchi H, Kashima T, Arakawa H. Significant influence of TiO2 photoelectrode morphology on the energy conversion efficiency of N719 dye- sensitized solar cell. Coord Chem Rev 2004; 248: 1381–9.

[80] Jafarzadeh M, Sipaut CS, Dayou J, Mansa RF. Recent progresses in solar cells: insight into hollow micro/nano–structures. Renew Sustain Energy Rev 2016; 64: 543–68.

[81] Bagheri S, Hir ZAM, Yousefi AT, Hamid SBA. Progress on mesoporous titanium dioxide: synthesis, modification and applications. Microporous Mesoporous Mater 2015; 218: 206–22.

[82] Muniz E, Goes M, Silva J, Varela JA, Joanni E, Parra R, et al. Synthesis and characterization of mesoporous TiO2 nanostructured films prepared by a modified sol–gel method for application in dye solar cells. Ceram Int 2011; 37: 1017–24.

[83] Sauvage F, Chen D, Comte P, Huang F, Heiniger L-P, Cheng Y-B, et al. Dye-sensitized solar cells employing a single film of mesoporous TiO2 beads achieve power conversion efficiencies over 10%. ACS Nano 2010; 4: 4420–5.

[84] Cao K, Lu J, Li H, Shen Y, Wang M. Efficient dye-sensitized solar cells using mesoporous submicrometer TiO2 beads. RSC Adv 2015; 5: 62630–7.

[85] Feng X, Zhu K, Frank AJ, Grimes CA, Mallouk TE. Rapid charge transport in dye sensitized solar cells made from vertically aligned single crystal rutile TiO2 nanowires. Angew Chem 2012; 124: 2781–4.

[86] Feng X, Shankar K, Varghese OK, Paulose M, Latempa TJ, Grimes CA. Vertically aligned single crystal TiO2 nanowire arrays grown directly on transparent conducting oxide coated glass: synthesis details and applications. Nano Lett 2008; 8: 3781–6.

[87] Wang H, Liu Y, Li M, Huang H, Zhong M, Shen H. Hydrothermal growth of large- scale macroporous TiO2 nanowires and its application in 3D dye-sensitized solar cells. Appl Phys A 2009; 97: 25–9.

[88] Adachi M, Murata Y, Takao J, Jiu J, Sakamoto M, Wang F. Highly efficient dye- sensitized solar cells with a titania thin-film electrode composed of a network structure of single-crystal-like TiO2 nanowires made by the "oriented attachment" mechanism. J Am Chem Soc 2004; 126: 14943–9.

[89] Lee B, Kim JI, Lee S, Hwang T, Nam S, Choi H, et al. Oriented hierarchical porous TiO2 nanowires on Ti substrate: evolution of nanostructures for dye-sensitized solar cells. Electrochim Acta 2014; 145: 231–6.

[90] Wu W-Q, Rao H-S, Xu Y-F, Wang Y-F, Su C-Y, Kuang D-B. Hierarchical oriented anatase TiO2 nanostructure arrays on flexible substrate for efficient dye-sensitized solar cells. Sci Rep; 3; 2013. p.1892.

[91] Fan J, FaÌbrega C, Zamani RR, Hao Y, Parra A, Andreu T, et al. Enhanced photovoltaic performance of nanowire dye-sensitized solar cells based on coaxial TiO2@TiO heterostructures with a cobalt (II/III) redox electrolyte. ACS Appl Mater Interfaces 2013; 5: 9872–7.

[92] Sun P, Zhang X, Wang C, Wei Y, Wang L, Liu Y. Rutile TiO2 nanowire array infiltrated with anatase nanoparticles as photoanode for dye-sensitized solar cells: enhanced cell performance via the rutile–anatase heterojunction. J Mater Chem A 2013; 1: 3309–14.

[93] Sun P, Zhang X, Wang L, Li F, Wei Y, Wang C, et al. Bilayer TiO2 photoanode consisting of a nanowire–nanoparticle bottom layer and a spherical voids scattering layer for dye-sensitized solar cells. New J Chem 2015; 39: 4845–51.

[94] Mor GK, Varghese OK, Paulose M, Shankar K, Grimes CA. A review on highly ordered, vertically oriented TiO2 nanotube arrays: fabrication, material proper- ties, and solar energy applications. Sol Energy Mater Sol Cells 2006; 90: 2011–75.

[95] Zhou Q, Fang Z, Li J, Wang M. Applications of TiO2 nanotube arrays in environmental and energy fields: a review. Microporous Mesoporous Mater 2015; 202: 22–35.

[96] Flores IC, de Freitas JN, Longo C, De Paoli M-A, Winnischofer H, Nogueira AF. Dye-sensitized solar cells based on TiO2 nanotubes and a solid-state electrolyte. J Photochem Photobiol A: Chem 2007; 189: 153–60.

[97] Park H, Kim W-R, Jeong H-T, Lee J-J, Kim H-G, Choi W-Y. Fabrication of dye- sensitized solar cells by transplanting highly ordered TiO2 nanotube arrays. Sol Energy Mater Sol Cells 2011; 95: 184–9.

[98] Wang S, Zhang J, Chen S, Yang H, Lin Y, Xiao X, et al. Conversion enhancement of flexible dye-sensitized solar cells based on TiO2 nanotube arrays with TiO2 nanoparticles by electrophoretic deposition. Electrochim Acta 2011; 56: 6184–8.

[99] Pavasupree S, Ngamsinlapasathian S, Nakajima M, Suzuki Y, Yoshikawa S. Synthesis, characterization, photocatalytic activity and dye-sensitized solar cell performance of nanorods/nanoparticles TiO2 with mesoporous structure. J Photochem Photobiol A: Chem 2006; 184: 163–9.

[100] Liu Z, Misra M. Dye-sensitized photovoltaic wires using highly ordered TiO2 nanotube arrays. ACS Nano 2010; 4: 2196–200.

[101] Dadgostar S, Tajabadi F, Taghavinia N. Mesoporous submicrometer TiO2 hollow spheres as scatterers in dye-sensitized solar cells. ACS Appl Mater Interfaces 2012; 4: 2964–8.

[102] Yang SC, Yang DJ, Kim J, Hong JM, Kim HG, Kim ID, et al. Hollow TiO2 hemispheres obtained by colloidal templating for application in dye sensitized solar Cells. Adv Mater 2008; 20: 1059–64.

[103] Tsai M-C, Lee J-Y, Chang Y-C, Yang M-H, Chen T-T, Chang I-C, et al. Scattering resonance enhanced dye absorption of dye sensitized solar cells at optimized hollow structure size. J Power Sources 2014; 268: 1–6.

[104] Yu J, Fan J, Lv K. Anatase TiO2 nanosheets with exposed (001) facets: improved photoelectric conversion efficiency in dye-sensitized solar cells. Nanoscale 2010; 2: 2144–9.

[105] Ramanathan T, Abdala A, Stankovich S, Dikin D, Herrera-Alonso M, Piner R, et al. Functionalized graphene sheets for polymer nanocomposites. Nat Nanotechnol 2008; 3: 327–31.

[106] Yang N, Zhai J, Wang D, Chen Y, Jiang L. Two-dimensional graphene bridges en- hanced photoinduced charge transport in dye-sensitized solar cells. ACS Nano 2010; 4: 887–94.

[107] Wang H, Leonard SL, Hu YH. Promoting effect of graphene on dye-sensitized solar cells. Ind Eng Chem Res 2012; 51: 10613–20.

[108] Tang Y-B, Lee C-S, Xu J, Liu Z-T, Chen Z-H, He Z, et al. Incorporation of graphenes in nanostructured TiO2 films via molecular grafting for dye-sensitized solar cell appli- cation. ACS Nano 2010; 4: 3482–8.

[109] Park J-H, Seo S-W, Kim J-H, Choi C-J, Kim H, Lee DK, et al. Improved efficiency of dye-sensitized solar cell using graphene-coated Al2O3-TiO2 nanocomposite photoanode. Mol Cryst Liq Cryst 2011; 538: 285–91.

[110] Tsai T-H, Chiou S-C, Chen S-M. Enhancement of dye-sensitized solar cells by using graphene–TiO2 composites as photoelectrochemical working electrode. Int J Electrochem Sci 2011; 6: 3333–43.

[111] Sun S, Gao L, Liu Y. Enhanced dye-sensitized solar cell using graphene–TiO2 photoanode prepared by heterogeneous coagulation. Appl Phys Lett 2010; 96: 3113.

[112] Kim A-Y, Kim J, Kim MY, Ha SW, Tien NTT, Kang M. Photovoltaic efficiencies on dye-sensitized solar cells assembled with graphene-linked TiO2 anode films. Bull Korean Chem Soc 2012; 33: 3355.

[113] TangB,HuG.Twokindsofgraphene-basedcompositesforphotoanodeapplyingin dye-sensitized solar cell. J Power Sources 2012; 220: 95–102.

[114] Fang X, Li M, Guo K, Zhu Y, Hu Z, Liu X, et al. Improved properties of dye-sensitized solar cells by incorporation of graphene into the photoelectrodes. Electrochim Acta 2012; 65: 174–8.

[115] de los Santos DM, Aguilar T, Saìnchez-Coronilla A, Navas J, Cruz Hernaìndez N, Alcantara R, et al. Electronic and structural properties of highly aluminum ion doped TiO2 nanoparticles: a combined experimental and theoretical study. ChemPhysChem 2014; 15: 2267–80.

[116] Zhang H, Lv X, Li Y, Wang Y, Li J. P25-graphene composite as a high performance photocatalyst. ACS Nano 2009; 4: 380–6.

[117] Zhang Y, Tang Z-R, Fu X, Xu Y-J. Engineering the unique 2D mat of graphene to achieve graphene–TiO2 nanocomposite for photocatalytic selective transformation: what advantage does graphene have over its forebear carbon nanotube? ACS Nano 2011; 5: 7426–35.

[118] Li Y, Wang G, Pan K, Jiang B, Tian C, Zhou W, et al. NaYF4: Er3+/Yb3+–graphene composites: preparation, upconversion luminescence, and application in dye- sensitized solar cells. J Mater Chem 2012; 22: 20381–6.

[119] YangH,GuoC,GuaiGH,SongQ,JiangSP,LiCM.Reductionofchargerecombination by an amorphous titanium oxide interlayer in layered graphene/quantum dots photochemical cells. ACS Appl Mater Interfaces 2011; 3: 1940–5.

[120] Liu X, Pan L, Lv T, Zhu G, Sun Z, Sun C. Microwave-assisted synthesis of CdS– reduced graphene oxide composites for photocatalytic reduction of Cr (vi). Chem Commun 2011; 47: 11984–6.

[121] Chappel S, Chen S-G, Zaban A. TiO2-coated nanoporous SnO2 electrodes for dye- sensitized solar cells. Langmuir 2002; 18: 3336–42.

[122] Neo CY, Ouyang J. Ethyl cellulose and functionalized carbon nanotubes as a co- gelator for high-performance quasi-solid state dye-sensitized solar cells. J Mater Chem 2013; 1: 14392–401.

[123] Nazeeruddin MK, Zakeeruddin S, Humphry-Baker R, Jirousek M, Liska P, Vlachopoulos N, et al. Acid-base equilibria of (2, 22 -bipyridyl-4, 42 -dicarboxylic acid) ruthenium (II) complexes and the effect of protonation on charge-transfer sensitization of nanocrystalline titania. Inorg Chem 1999; 38: 6298–305.

[124] Mak KF, Sfeir MY, Wu Y, Lui CH, Misewich JA, Heinz TF. Measurement of the optical conductivity of graphene. Phys Rev Lett 2008; 101: 196405.

[125] Long R, English NJ, Prezhdo OV. Photo-induced charge separation across the graphene–TiO2 interface is faster than energy losses: a time-domain ab initio anal- ysis. J Am Chem Soc 2012; 134: 14238–48.

[126] Zhang Y, Zhang N, Tang Z-R, Xu Y-J. Graphene transforms wide band gap ZnS to a visible light photocatalyst. The new role of graphene as a macromolecular photo- sensitizer. ACS Nano 2012; 6: 9777–89.

[127] Williams KJ, Nelson CA, Yan X, Li L-S, Zhu X. Hot electron injection from graphene quantum dots to TiO2. ACS Nano 2013; 7: 1388–94.

[129] Velten JA, Carretero-Gonzaìlez J, Castillo-Martiìnez E, Bykova J, Cook A, Baughman R, et al. Photoinduced optical transparency in dye-sensitized solar cells containing graphene nanoribbons. J Phys Chem C 2011; 115: 25125–31.

[130] Ahmad I, Khan U, Gun'ko YK. Graphene, carbon nanotube and ionic liquid mix- tures: towards new quasi-solid state electrolytes for dye sensitised solar cells. J Mater Chem 2011; 21: 16990–6.

[131] Oregan B, Gratzel M. A low-cost, high-efficiency solar-cell based on dye-sensitized colloidal TiO2 films. Nature 1991; 353: 737–40.

[132] Zhang DW, Li XD, Li HB, Chen S, Sun Z, Yin XJ, et al. Graphene-based counter elec- trode for dye-sensitized solar cells. Carbon 2011; 49: 5382–8.

[133] Kaniyoor A, Ramaprabhu S. Thermally exfoliated graphene based counter electrode for low cost dye sensitized solar cells. J Appl Phys 2011; 109.

[134] Hsieh CT, Yang BH, Lin JY. One- and two-dimensional carbon nanomaterials as counter electrodes for dye-sensitized solar cells. Carbon 2011; 49: 3092–7.

[135] Cruz R, Tanaka DAP, Mendes A. Reduced graphene oxide films as transparent counter-electrodes for dye-sensitized solar cells. Sol Energy 2012; 86: 716–24. [65] Wan L, Wang SM, Wang XB, Dong BH, Xu ZX, Zhang XH, et al. Room-temperature fabrication of graphene films on variable substrates and its use as counter elec-trodes for dye-sensitized solar cells. Solid State Sci 2011; 13: 468–75.

[136] Dou YY, Li GR, Song J, Gao XP. Nickel phosphide-embedded graphene as counter electrode for dye-sensitized solar cells. Phys Chem Chem Phys 2012; 14: 1339–42.

[137] Mei XG, Cho SJ, Fan BH, Ouyang JY. High-performance dye-sensitized solar cells with gel-coated binder-free carbon nanotube films as counter electrode. Nanotech- nology 2010; 21.

[140] Chou CS, Huang CI, Yang RY, Wang CP. The effect of SWCNT with the functional group deposited on the counter electrode on the dye-sensitized solar cell. Adv Powder Technol 2010; 21: 542–50.

[141] Imoto K, Takahashi K, Yamaguchi T, Komura T, Nakamura J, Murata K. High- performance carbon counter electrode for dye-sensitized solar cells. Sol Energy Mater Sol Cells 2003; 79: 459–69.

[142] Dong P, Pint CL, Hainey M, Mirri F, Zhan YJ, Zhang J, et al. Vertically aligned single- walled carbon nanotubes as low-cost and high electrocatalytic counter electrode for dye-sensitized solar cells. ACS Appl Mater Interfaces 2011; 3: 3157–61.

[143] Hao F, Dong P, Zhang J, Zhang YC, Loya PE, Hauge RH, et al. High electrocatalytic ac- tivity of vertically aligned single-walled carbon nanotubes towards sulfide redox shuttles. Sci Rep 2012; 2.

[144] Lee KS, Lee WJ, Park NG, Kim SO, Park JH. Transferred vertically aligned N-doped carbon nanotube arrays: use in dye-sensitized solar cells as counter electrodes. Chem Commun 2011; 47: 4264–6.

[145] Choi H, Kim H, Hwang S, Choi W, Jeon M. Dye-sensitized solar cells using graphene- based carbon nano composite as counter electrode. Sol Energ Mat Sol Cells 2011; 95: 323–5.

[146] Choi H, Kim H, Hwang S, Kang M, Jung DW, Jeon M. Electrochemical electrodes of graphene-based carbon nanotubes grown by chemical vapor deposition. Scr Mater 2011; 64: 601–4.

[147] Zhu G, Pan LK, Lu T, Xu T, Sun Z. Electrophoretic deposition of reduced graphene- carbon nanotubes composite films as counter electrodes of dye-sensitized solar cells. J Mater Chem 2011; 21: 14869–75.

[148] Battumur T, Mujawar SH, Truong QT, Ambade SB, Lee DS, Lee W, et al. Graphene/ carbon nanotubes composites as a counter electrode for dye-sensitized solar cells. Curr Appl Phys 2012; 12: E49–53.

[149] Velten J, Mozer A, Li D, Officer D, Wallace G, Baughman R, et al. Carbon nanotube/ graphene nanocomposite as efficient counter electrodes in dye-sensitized solar cells. Nanotechnology 2012; 23 (085201).

[150] Dong P, Zhu Y, Zhang J, Hao F, Wu JJ, Lei SD, et al. Vertically aligned carbon nano- tubes/graphene hybrid electrode as a TCO- and Pt-free flexible cathode for applica- tion in solar cells. J Mater Chem A 2014; 2: 20902–7.

[151] Gong F, Wang H, Wang ZS. Self-assembled monolayer of graphene/Pt as counter electrode for efficient dye-sensitized solar cell. Phys Chem Chem Phys 2011; 13: 17676–82.

[152] Bajpai R, Roy S, Kumar P, Bajpai P, Kulshrestha N, Rafiee J, et al. Graphene support- ed platinum nanoparticle counter-electrode for enhanced performance of dye- sensitized solar cells. ACS Appl Mater Interfaces 2011; 3: 3884–9.

[153] Yen MY, Teng CC, Hsiao MC, Liu PI, Chuang WP, Ma CCM, et al. Platinum nanopar- ticles/graphene composite catalyst as a novel composite counter electrode for high performance dye-sensitized solar cells. J Mater Chem 2011; 21: 12880–8.

[154] Hong WJ, Xu YX, Lu GW, Li C, Shi GQ. Transparent graphene/PEDOT-PSS composite films as counter electrodes of dye-sensitized solar cells. Electrochem Commun 2008; 10: 1555–8.

[155] Wang GQ, Zhuo SP, Xing W. Graphene/polyaniline nanocomposite as counter elec- trode of dye-sensitized solar cells. Mater Lett 2012; 69: 27–9.

[156] Lee KS, Lee Y, Lee JY, Ahn JH, Park JH. Flexible and platinum-free dye-sensitized solar cells with conducting-polymer-coated graphene counter electrodes. ChemSusChem 2012; 5: 379–82.

[157] Wang GQ, Xing W, Zhuo SP. The production of polyaniline/graphene hybrids for use as a counter electrode in dye-sensitized solar cells. Electrochim Acta 2012; 66: 151–7.

[158] Gong F, Xu X, Zhou G, Wang ZS. Enhanced charge transportation in a polypyrrole counter electrode via incorporation of reduced graphene oxide sheets for dye- sensitized solar cells. Phys Chem Chem Phys 2013; 15: 546–52.

[159] Kaniyoor A, Ramaprabhu S. Soft functionalization of graphene for enhanced tri- iodide reduction in dye sensitized solar cells. J Mater Chem 2012; 22: 8377–84.

[160] Li SS, Luo YH, Lv W, Yu WJ, Wu SD, Hou PX, et al. Vertically aligned carbon nano- tubes grown on graphene paper as electrodes in lithium-ion batteries and dye- sensitized solar cells. Adv Energy Mater 2011; 1: 486–90.

[161] Hardin BE, Snaith HJ, McGehee MD. The renaissance of dye-sensitized solar cells. Nat Photonics 2012; 6: 162–9.

[162] WangP,ZakeeruddinSM,MoserJE,NazeeruddinMK,SekiguchiT,GratzelM.Asta-ble quasi-solid-state dye-sensitized solar cell with an amphiphilic ruthenium sen-sitizer and polymer gel electrolyte. Nat Mater 2003; 2: 402–7.

[163] Wang P, Zakeeruddin SM, Comte P, Exnar I, Gratzel M. Gelation of ionic liquid- based electrolytes with silica nanoparticles for quasi-solid-state dye-sensitized solar cells. J Am Chem Soc 2003; 125: 1166–7.

[164] Li S, Qiu L, Shi C, Chen X, Yan F. Water resistant, solid state, dye sensitized solar cells based on hydrophobic organic ionic plastic crystal electrolytes. Adv Mater 2014; 26: 1266–71.

[165] Zhang W, Yuan C, Guo J, Qiu L, Yan F. Supramolecular ionic liquid gels for quasi-solid-state dye-sensitized solar cells. ACS Appl Mater Interfaces 2014; 6: 8723–8.

[166] Shi C, Li S, Zhang W, Qiu L, Yan F. Bis-quaternary ammonium cation-based organic ionic plastic crystals: plastic crystal behaviour and ionic liquid properties above melting points. J Mater Chem A 2013; 1: 13956–62.

[167] Li G, Song J, Pan G, Gao X. Highly Pt-like electrocatalytic activity of transition metal nitrides for dye-sensitized solar cells. Energy Environ Sci 2011; 4: 1680–3.

[168] Wang X, Zhi L, Mullen K. Transparent, conductive graphene electrodes for dye-sensitized solar cells. Nano Lett 2008; 8: 323–7.

[169] Suzuki K, Yamaguchi M, Kumagai M, Yanagida S. Application of carbon nanotubes to counter electrodes of dye-sensitized solar cells. Chem Lett 2003; 32: 28–9.

[170] Zheng X, Deng J, Wang N, Deng D, Zhang WH, Bao X, et al. Podlike N doped carbon nanotubes encapsulating FeNi alloy nanoparticles: high performance counter elec- trode materials for dye sensitized solar cells. Angew Chem Int Ed 2014; 53: 7023–7.

[171] Du X, Skachko I, Barker A, Andrei EY. Approaching ballistic transport in suspended graphene. Nat Nanotechnol 2008; 3: 491–5.

[172] Unarunotai S, Murata Y, Chialvo CE, Mason N, Petrov I, Nuzzo RG, et al. Conjugated carbon monolayer membranes: methods for synthesis and integration. Adv Mater2010; 22: 1072–7.

[173] Peigney A, Laurent C, Flahaut E, Bacsa R, Rousset A. Specific surface area of carbon nanotubes and bundles of carbon nanotubes. Carbon 2001; 39: 507–14.

[174] Nair R, Blake P, Grigorenko A, Novoselov K, Booth T, Stauber T, et al. Fine structure constant defines visual transparency of graphene. Science 2008; 320 (1308-).

[175] Du J, Lai X, Yang N, Zhai J, Kisailus D, Su F, et al. Hierarchically ordered macro– mesoporous TiO2–graphene composite films: improved mass transfer, reduced charge recombination, and their enhanced photocatalytic activities. ACS Nano 2010; 5: 590–6.

[176] Yan X, Cui X, Li B, Li L-s. Large, solution-processable graphene quantum dots as light absorbers for photovoltaics. Nano Lett 2010; 10: 1869–73.

[177] Chen T, Hu W, Song J, Guai GH, Li CM. Interface functionalization of photoelectrodes with graphene for high performance dye sensitized solar cells.Adv Funct Mater 2012; 22: 5245–50.

[178] Ng YH, Lightcap IV, Goodwin K, Matsumura M, Kamat PV. To what extent do graphene scaffolds improve the photovoltaic and photocatalytic response of TiO2 nanostructured films? J Phys Chem Lett 2010; 1: 2222–7.

[179] Peining Z, Nair AS, Shengjie P, Shengyuan Y, Ramakrishna S. Facile fabrication of TiO2–graphene composite with enhanced photovoltaic and photocatalytic proper-ties by electrospinning. ACS Appl Mater Interfaces 2012; 4: 581–5.

[180] JungM-H,KangMG,ChuM-J.Iodide-functionalizedgrapheneelectrolyteforhighly efficient dye-sensitized solar cells. J Mater Chem 2012; 22: 16477–83.

[181] Roy-Mayhew JD, Bozym DJ, Punckt C, Aksay IA. Functionalized graphene as a cata-lytic counter electrode in dye-sensitized solar cells. ACS Nano 2010; 4: 6203–11.

[182] Neto AC, Guinea F, Peres N, Novoselov KS, Geim AK. The electronic properties of graphene. Rev Mod Phys 2009; 81: 109.

[183] Geim AK. Graphene: status and prospects. Science 2009; 324: 1530–4.

[184] Xu M, Liang T, Shi M, Chen H. Graphene-like two-dimensional materials. Chem Rev 2013; 113: 3766–98.

[185] Chopra K, Major S, Pandya D. Transparent conductors—a status review. Thin Solid Films 1983; 102: 1–46.

[186] Bonaccorso F, Sun Z, Hasan T, Ferrari A. Graphene photonics and optoelectronics. Nat Photonics 2010; 4: 611–22.

[187] Bi H, Sun S, Huang F, Xie X, Jiang M. Direct growth of few-layer graphene films on SiO2 substrates and their photovoltaic applications. J Mater Chem 2012; 22: 411–6.

[188] Kim SR, Parvez MK, Chhowalla M. UV-reduction of graphene oxide and its applica- tion as an interfacial layer to reduce the back-transport reactions in dye-sensitized solar cells. Chem Phys Lett 2009; 483: 124–7.

[189] Jarernboon W, Pimanpang S, Maensiri S, Swatsitang E, Amornkitbamrung V. Effects of multiwall carbon nanotubes in reducing microcrack formation on electrophoretically deposited TiO2 film. J Alloy Compd 2009; 476: 840–6.

[190] Naim MN, Iijima M, Kamiya H, Lenggoro IW. Electrophoretic packing structure from aqueous nanoparticle suspension in pulse DC charging. Colloids Surf A: Physicochem Eng Asp 2010; 360: 13–9.

[191] Tang Y-B, Lee C-S, Xu J, Liu Z-T, Chen Z-H, He Z, et al. Incorporation of graphenes in nanostructured TiO2 films via molecular grafting for dye-sensitized solar cell application. ACS Nano 2010; 4: 3482–8.

[192] Benehkohal NP, Demopoulos G. Green preparation of TiO2-ZnO nanocomposite photoanodes by aqueous electrophoretic deposition. J Electrochem Soc 2012; 159: B602–B610.

[193] Grinis L, Kotlyar S, Ruhle S, Grinblat J, Zaban A. Conformal nano sized inorganic coatings on mesoporous TiO2 films for low temperature dye sensitized solar cell fabrication. Adv Funct Mater 2010; 20: 282–8.

[194] Jiang C, Leung MY, Koh WL, Li Y. Influences of deposition and post-annealing temperatures on properties of TiO2 blocking layer prepared by spray pyrolysis for solid-state dye-sensitized solar cells. Thin Solid Films 2011; 519: 7850–4.

[195] Okuya M, Nakade K, Kaneko S. Porous TiO2 thin films synthesized by a spray pyrolysis deposition (SPD) technique and their application to dye-sensitized solar cells. Sol Energy Mater Sol Cells 2002; 70: 425–35.

[196] Bandara H, Rajapakse R, Murakami K, Kumara G, Sepalage GA. Dye-sensitized solar cell based on optically transparent TiO2 nanocrystalline electrode prepared by atomized spray pyrolysis technique. Electrochim Acta 2011; 56: 9159–61.

[197] Jiu J, Wang F, Sakamoto M, Takao J, Adachi M. Performance of dye-sensitized solar cell based on nanocrystals TiO2 film prepared with mixed template method. Sol Energy Mater Sol Cells 2005; 87: 77–86.

[198] Alexaki N, Stergiopoulos T, Kontos A, Tsoukleris D, Katsoulidis A, Pomonis P, et al. Mesoporous titania nanocrystals prepared using hexadecylamine surfactant template: crystallization progress monitoring, morphological characterization and application in dye-sensitized solar cells. Microporous Mesoporous Mater 2009; 124: 52–8.

[199] Yun TK, Park SS, Kim D, Hwang Y-K, Huh S, Bae JY, et al. Pore-size effect on photovoltaic performance of dye-sensitized solar cells composed of mesoporous anatase-titania. J Power Sources 2011; 196: 3678–82.

[200] Liu Y, Wang S, Shan Z, Li X, Tian J, Mei Y, et al. Anatase TiO2 hollow spheres with small dimension fabricated via a simple preparation method for dye-sensitized solar cells with an ionic liquid electrolyte. Electrochim Acta 2012; 60: 422–7.

[201] Qi L, Birnie DP. Templated titania films with meso-and macroporosities. Mater Lett 2007; 61: 2191–4.

[202] Liu Z, Liu C, Ya J, Lei E. Controlled synthesis of ZnO and TiO2 nanotubes by chemical method and their application in dye-sensitized solar cells. Renew Energy 2011; 36: 1177–81.

[203] Han C-C, Ho S-Y, Lin Y-P, Lai Y-C, Liang W-C, Chen-Yang Y-W. Effect of π–π stacking of water miscible ionic liquid template with different cation chain length and content on morphology of mesoporous TiO2 prepared via sol–gel method and the applications. Microporous Mesoporous Mater 2010; 131: 217–23.

[204] Trancik JE. Energy: photovoltaics-a niche-market distraction or a global energy solution?. Geo Public Pol'Y Rev 2006; 11: 69–119.

[205] S'en Z. Solar energy fundamentals and modeling techniques: atmosphere, envir- onment, climate change and renewable energy. London: Springer; 2008.

[206] Duarte D, Massi M, Maciel H, da Silva Sobrinho A, Braga T, Moraes R, et al. Dye- sensitized solar cells: a new benchmark for electric power generation in Brazil. In: Proceedings of the IEEE world congress on sustainable technologies (WCST); 2012. p. 117.

[207] Matiko J, Grabham N, Beeby S, Tudor M. Review of the application of energy harvesting in buildings. Meas Sci Technol 2013; 25: 012002.

[208] Nielsen TD, Cruickshank C, Foged S, Thorsen J, Krebs FC. Business, market and intellectual property analysis of polymer solar cells. Sol Energy Mater Sol Cells 2010; 94: 1553–71.

[209] Global E-paper. Display market by manufacturers, countries, type and application, forecast to 2022; 2017. p. 117.

[210] Miyasaka T, Kijitori Y, Ikegami M. Plastic dye-sensitized photovoltaic cells and modules based on low-temperature preparation of mesoscopic titania electrodes. Electrochemistry 2007; 75: 2–12.

[211] Ramasamy E, Lee WJ, Lee DY, Song JS. Spray coated multi-wall carbon nanotube counter electrode for tri-iodide reduction in dye-sensitized solar cells. Electrochem Commun 2008; 10: 1087–9.

[212] Mozaffari S, Nateghi MR, Zarandi MB. An overview of the challenges in the commercialization of dye sensitized solar cells. Renew Sustain Energy Rev 2016. Ando Y, Kindole D, Noda Y, Mbiu RN, Kosgey BK, Maranga SM, et al. Alumina and titania films deposition by APS/ASPPS dual mode thermal spray equipment using Ar added N2 working gas. Vacuum 2017; 136: 203–8.

[213] Meng L, Ren T, Li C. The control of the diameter of the nanorods prepared by dc reactive magnetron sputtering and the applications for DSSC. Appl Surf Sci 2010; 256: 3676–82.

[214] Senthilkumar V, Jayachandran M, Sanjeeviraja C. Preparation of anatase TiO2 thin films for dye-sensitized solar cells by DC reactive magnetron sputtering technique. Thin Solid Films 2010; 519: 991–4.

[215] Wu S, Han H, Tai Q, Zhang J, Xu S, Zhou C, et al. Improvement in dye-sensitized solar cells employing TiO2 electrodes coated with Al2O3 by reactive direct current magnetron sputtering. J Power Sources 2008; 182: 119–23.

[216] Jin Y-S, Kim K-H, Kim W-J, Jang K-U, Choi H-W. The effect of RF-sputtered TiO2 passivating layer on the performance of dye sensitized solar cells. Ceram Int 2012; 38: S505–S509.

[217] Kang SH, Kang M-S, Kim H-S, Kim J-Y, Chung Y-H, Smyrl WH, et al. Columnar rutile TiO2 based dye-sensitized solar cells by radio-frequency magnetron sputtering. J Power Sources 2008; 184: 331–5.

[218] Garcia EM, Lins VF, Matencio T. Metallic and oxide electrodeposition. Mod Surf Eng Treat InTech 2013.

[219] Saelim N-O, Magaraphan R, Sreethawong T. Preparation of sol–gel TiO2/purified Na-bentonite composites and their photovoltaic application for natural dye- sensitized solar cells. Energy Convers Manag 2011; 52: 2815–8.

[220] Hartnagel H, Dawar A, Jain A, Jagadish C. Semiconducting transparent thin films. UK: Institute of Physics Bristol, Taylor and Francis; 1995.

[221] Johnson RW, Hultqvist A, Bent SF. A brief review of atomic layer deposition: from fundamentals to applications. Mater Today 2014; 17: 236–46.

[222] Chen Y, Lo Y, Huang C, Cai Y, Hsu M. Anode growth of DSSCs by flat-flame chemical vapor deposition method. Mater Chem Phys 2010; 120: 181–6.

[223] Kim KE, Jang S-R, Park J, Vittal R, Kim K-J. Enhancement in the performance of dye-sensitized solar cells containing ZnO-covered TiO2 electrodes prepared by thermal chemical vapor deposition. Sol Energy Mater Sol Cells 2007; 91: 366–70.

[224] Nam SH, Hyun J-S, Boo J-H. Synthesis of TiO2 thin films using single molecular precursors by MOCVD method for dye-sensitized solar cells application and study on film growth mechanism. Mater Res Bull 2012; 47: 2717–21.

[225] Nejati S, Lau KK. Integration of polymer electrolytes in dye sensitized solar cells by initiated chemical vapor deposition. Thin Solid Films 2011; 519: 4551–4.

[226] Quinonez C, Vallejo W, Gordillo G. Structural, optical and electrochemical properties of TiO2 thin films grown by APCVD method. Appl Surf Sci 2010; 256: 4065–71.

[227] Shinde P, Bhosale C. Properties of chemical vapour deposited nanocrystalline TiO2 thin films and their use in dye-sensitized solar cells. J Anal Appl Pyrolysis 2008; 82: 83–8.

[228] Ganapathy V, Karunagaran B, Rhee S-W. Improved performance of dye-sensitized solar cells with TiO2/alumina core–shell formation using atomic layer deposition. J Power Sources 2010; 195: 5138–43.

[229] Lee J, Hong KS, Shin K, Jho JY. Fabrication of dye-sensitized solar cells using ordered and vertically oriented TiO2 nanotube arrays with open and closed ends. J Ind Eng Chem 2012; 18: 19–23.

[230] Tien T-C, Pan F-M, Wang L-P, Tsai F-Y, Lin C. Growth mode transition of atomic layer deposited Al2O3 on porous TiO2 electrodes of dye-sensitized solar cells. Thin Solid Films 2012; 520: 1745–50.

[231] Tsai T-Y, Lu S-Y. A novel way of improving light harvesting in dye-sensitized solar cells–electrodeposition of titania. Electrochem Commun 2009; 11: 2180–3.

Xie Y-L, Li Z-X, Xu Z-G, Zhang H-L. Preparation of coaxial TiO2/ZnO nanotube arrays for high-efficiency photo-energy conversion applications. Electrochem Commun 2011; 13: 788–91.

[232] An H-J, Jang S-R, Vittal R, Lee J, Kim K-J. Cationic surfactant promoted reductive electrodeposition of nanocrystalline anatase TiO2 for application to dye- sensitized solar cells. Electrochim Acta 2005; 50: 2713–8.

[234] Wessels K, Maekawa M, Rathousky J, Oekermann T. One-step electrodeposition of TiO2/dye hybrid films. Thin Solid Films 2007; 515: 6497–500.

[235] Zhao L, Yu J, Fan J, Zhai P, Wang S. Dye-sensitized solar cells based on ordered titanate nanotube films fabricated by electrophoretic deposition method. Electrochem Commun 2009; 11: 2052–5.

[236] Chen H-W, Huang K-C, Hsu C-Y, Lin C-Y, Chen J-G, Lee C-P, et al. Electrophoretic deposition of TiO2 film on titanium foil for a flexible dye- sensitized solar cell. Electrochim Acta 2011; 56: 7991–8.

[237] Tsai C-C, Chu Y-Y, Teng H. A simple electrophoretic deposition method to prepare TiO2–B nanoribbon thin films for dye-sensitized solar cells. Thin Solid Films 2010; 519: 662–5.

[238] Chen H-W, Hsu C-Y, Chen J-G, Lee K-M, Wang C-C, Huang K-C, et al. Plastic dye- sensitized photo-supercapacitor using electrophoretic deposition and compression methods. J Power Sources 2010; 195: 6225–31.

[239] Sadeghi A, Ebadzadeh T, Raissi B, Ghashghaie S, Fateminia S. Application of the multi-step EPD technique to fabricate thick TiO2 layers: effect of organic medium viscosity on the layer microstructure. J Phys Chem B 2013; 117: 1731–7.

[240] Molina T, Vicent M, Saìnchez E, Moreno R. Stability and EPD of concentrated suspensions of alumina with nanosized titania. Key Eng Mater: Trans Tech Publ 2012: 203–7.